Contents lists available at ScienceDirect

Arabian Journal of Chemistry

journal homepage: www.ksu.edu.sa

Original article

Phytochemical composition and anticancer effect of *Akebia trifoliata* seed in non-small cell lung cancer A549 cells

Yuanquan Ran [a,b], Lanlan Yang [b], Xiaoyan Jia [b], Huan Zhao [b], Qiong Hu [a], Bing Yang [a], Dongxin Tang [a,*], Minyi Tian [a,b,*]

[a] *First Affiliated Hospital of Guizhou University of Traditional Chinese Medicine, Guiyang 550000, China*
[b] *National & Local Joint Engineering Research Center for the Exploitation of Homology Resources of Southwest Medicine and Food, Guizhou University, Guiyang 550025, China*

ARTICLE INFO

Keywords:
Akebia trifoliata
Phytochemical compounds
Lung cancer
Proliferation
Apoptosis
Migration and invasion

ABSTRACT

Background: Akebia trifoliata is a widely distributed medicine and food homology plant. Its fruit is used to treat tumors and the seed's weight proportion exceeds 50%. However, the anti-tumor effect of *A. trifoliata* seed remains poorly studied.

Methods: UHPLC-Q-Orbitrap-MS was used to identify the chemical components of *A. trifoliata* seed water extract (WE) and ethanolic extract (EE), and their cytotoxicity was evaluated using MTT assay. Further, colony formation and cell cycle assays examined the anti-proliferative effect of *A. trifoliata* seed EE. Next, morphology observation, AO/EB staining, Hoechst 33,258 staining, Annexin V-PE/7-AAD staining, and JC-1 assays were employed to detect apoptosis. The influence of *A. trifoliata* seed EE on A549 cell metastasis was assessed by wound healing and transwell invasion tests. In addition, western blotting and network pharmacology were applied to further analyze its anticancer mechanism.

Results: Eighty-two components were characterized from the *A. trifoliata* seed WE and EE. For anticancer activity, *A. trifoliata* seed EE exhibited high cytotoxicity against cancer cells A549 (IC_{50}: 52.38 ± 1.04 μg/mL) and NCI-H1299 (IC_{50}: 70.29 ± 0.58 μg/mL) and revealed low cytotoxicity against non-cancer cells MRC-5 (IC_{50}: 101.28 ± 2.84 μg/mL) and L929 (IC_{50}: 113.44 ± 0.55 μg/mL). *A. trifoliata* seed EE suppressed A549 cell proliferation by inducing S-phase arrest *via* down-regulation of CDK2 and p21 as well as up-regulation of cyclin E1 and E2. It increased the Bax/Bcl-2 ratio, reduced mitochondrial membrane potential (ΔΨm), activated caspase-9 and caspase-3, cleaved PARP, and triggered apoptosis through the mitochondrial pathway. Besides, it repressed migratory and invasive ability by reducing MMP-2, MMP-9, and N-cadherin levels.

Conclusion: A. trifoliata seed EE exhibits outstanding anticancer properties and has the exploitation potential as an anticancer drug in the pharmaceutical industry.

1. Introduction

Lung cancer accounts for 18 % of all cancer fatalities and is the primary cause of cancer-related mortality (Sung et al., 2021). As the most common type of lung cancer, non-small cell lung cancer (NSCLC) has a high incidence rate, accounting for 85 % of lung cancer incidence rates (Niu et al., 2024). Many of the anticancer drugs in clinical use today, like camptothecin, paclitaxel, and vinblastine, originated from plant-derived natural products (El-Hawary et al., 2022; Huang et al., 2021; Naeem et al., 2022). In addition, various plant extracts have been developed into clinical anticancer drugs in China, such as *Xiaoaiping* injection (*Marsdenia tenacissima* water extract), *Hedyotis diffusa* injection (*Hedyotis diffusa* ethanolic extract), and *Brucea javanica* oil soft capsule (*Brucea javanica* petroleum ether extract) (Huang et al., 2022; Zhang et al., 2018; Zhou et al., 2022a). Hence, plant-derived natural products are important sources for discovering anticancer drugs.

Akebia trifoliata (Thunb.) Koidz. belongs to the *Akebia* genus (Lardizabalaceae), which is extensively distributed throughout Asia, North America, and Europe and is especially cultivated in China as a highly valuable medicine and food homology plant (Chen and Tatemi, 2001;

* Corresponding authors at: D. Tang at First Affiliated Hospital of Guizhou University of Traditional Chinese Medicine, Guiyang 550000, China; M. Tian at National & Local Joint Engineering Research Center for the Exploitation of Homology Resources of Southwest Medicine and Food, Guizhou University, Guiyang 550025, China
E-mail addresses: dongxintang0319@163.com (D. Tang), mytian@gzu.edu.cn (M. Tian).

https://doi.org/10.1016/j.arabjc.2024.106020
Received 30 June 2024; Accepted 8 October 2024
Available online 14 October 2024

WFO, 2024; Zhou et al., 2017). *A. trifoliata* stem is used as a traditional medicine and is included in the official pharmacopeias of China, Europe, the United States, and Japan to treat damp-heat, amenorrhea, tongue sores, red urine, dysuria, edema, and stranguria (China Pharmacopoeia Committee, 2020; Guan et al., 2022; Li et al., 2023a; Maciąg et al., 2021). *A. trifoliata* stem is also utilized as cosmetic material, which is listed in the CosIng (Cosmetic Ingredient Database) of the European Commission and the "Catalogue of Cosmetic Raw Materials Used (2021 Edition)" approved by the China National Medical Products Administration (NMPA) (CosIng, 2024; Li et al., 2023b; NMPA, 2024). Its whole fruit, as a traditional Chinese medicine known as "*Yuzhizi*" (预知子), is also registered in the Chinese Pharmacopoeia to treat cancer, abdominal pain, dysmenorrhea, amenorrhea, and dysuria (China Pharmacopoeia Committee, 2020; Tang et al., 2020). *A. trifoliata* is consumed as a fruit in China and processed into fruit tea and wine because its pulp is soft and sweet and is rich in fiber, minerals, sugars, vitamins, crude proteins, and amino acids (Li et al., 2010; Zou et al., 2022). *A. trifoliate* pericarp is employed in preparing tea drinks, and the pectin derived from its pericarp can be exploited as a wound dressing (Sun et al., 2018; Yu et al., 2019). *A. trifoliata* seed accounts for a significant proportion of the weight of the whole fruit, ranging from 59.7 % to 83.4 %, which is utilized to extract oil and prepare skin creams and soaps (Jiang et al., 2020; Min et al., 2023; Su et al., 2021; Zhou et al., 2022b). Past research has shown that *A. trifoliata* stem containes lignans, phenylpropanoids, caffeoyl quinic acids, phenols, and triterpenoids (Liu et al., 2018b; Maciąg et al., 2021). The ethanol extract of *A. trifoliata* stem has been proven to suppress the cell viability of gastric cancer SGC-7901 cells (Lu et al., 2013). The seed of *A. trifoliata* contains triterpenoids, fatty acids, alkaloids, and flavonoids (Chen et al., 2022; Maciąg et al., 2021). The ethanol extract of *A. trifoliata* seed has been demonstrated to effectively inhibit the proliferation and metastasis of hepatocellular carcinoma cells (Lu et al., 2014; Lu et al., 2019). Moreover, several triterpenoids have been identified from *A. trifoliata* leaf and have been demonstrated to have cytotoxic activity to tumor cells (HeLa, HepG2, and A549) (Maciąg et al., 2021; Ouyang et al., 2018).

Lung cancer is the leading cause of cancer death, and plant-derived natural products are excellent sources of anti-lung cancer drugs. In particular, various plant extracts have been developed into clinical anticancer drugs in China. *A. trifoliata* fruit, its main medicinal part, has been used to treat tumors. *A. trifoliata* seed accounts for the majority of the fruit mass (59.7 % − 83.4 %) and is utilized to extract oil and prepare skin creams and soaps. However, *A. trifoliata* seed is usually discarded as waste (Zhang et al., 2024), and its anti-tumor effect remains poorly studied. Therefore, this study focused on the seed of *A. trifoliata*, aiming to study its anti-lung cancer properties and related mechanisms for the first time.

2. Materials and methods

2.1. Chemicals and reagents

Cell mitochondrial isolation kit, RIPA lysis buffer, JC-1 kit, and apoptosis Hoechst staining kit were from Beyotime Institute of Biotechnology (Shanghai, China). Aladdin Industrial Corporation (Shanghai, China) supplied cisplatin. Solarbio Life Sciences (Beijing, China) provided 0.1 % crystal violet solution, BCA protein assay kit, EB (ethidium bromide), AO (acridine orange), MTT solution, and 4 % paraformaldehyde. MultiSciences Biotech Co., Ltd (Hangzhou, China) provided Annexin V-PE/7-AAD apoptosis and cell cycle staining kits. Yeasen Biotechnology Co., Ltd (Shanghai, China) supplied the super ECL detection reagent. Cell Signaling Technology (Danvers, Massachusetts, USA) provided the antibodies. All other reagents are of analytical grade.

2.2. Plant material

A. trifoliata was harvested in August 2021 from Yuping County, Tongren District, Guizhou Province, China (27°14′20.1″N and 108°54′11.0″E). Prof. Guoxiong Hu confirmed the species of *A. trifoliata*, and the voucher specimen (herbarium code: AT20210827) was deposited at the College of Life Sciences, Guizhou University.

2.3. A. trifoliata seed EE and WE preparation

Fresh seed (500 g) of *A. trifoliata* was pulverized and placed in a 5L round-bottomed flask. Then, *A. trifoliata* seed ethanolic extract (EE) and water extract (WE) were prepared by reflux extraction with ethanol (70 %, 2L) at 80 °C for 2 h and distilled water (2L) at 100 °C for 2 h, respectively. Next, suction filtration was carried out to collect the filtrate. Subsequently, 70 % ethanol or distilled water (2 L) was added to the round-bottomed flask, and *A. trifoliata* seed filter residue was extracted again under reflux with ethanol (70 %, 2L) at 80 °C for 2 h or distilled water (2L) at 100 °C for 2 h. Then, we collected the second filtrate, combined the two filtrates, and used a rotary evaporator (60 °C) to concentrate samples. Subsequently, the concentrated samples were frozen in a −80 °C freezer for 72 h and freeze-dried using an LGJ-12 vacuum freeze dryer (Songyuan, Beijing, China) for 72 h to obtain *A. trifoliata* seed EE and WE. Finally, the desiccator was used to store the dried samples sealed in brown glass bottles.

2.4. Phytochemical analysis of A. trifoliata seed EE and WE

Phytochemicals in *A. trifoliata* seed EE and WE were analyzed using UHPLC-Q-Orbitrap-MS (ultra-high-performance liquid chromatography coupled with quadrupole orbitrap mass spectrometer). The parameters utilized for the Dionex Ultimate 3000 RSLC UHPLC were set as follows: column (100 mm × 2.1 mm, 1.9 μm, Thermo Fisher Hypersil GOLD aQ), mobile phase consisted of formic acid acetonitrile (A, 0.1 %) and formic acid aqueous solution (B, 0.1 %), injection volume (5 μL), flow rate (0.3 mL/min), and column temperature(40 °C). In order to separate *A. trifoliata* seed EE and WE components, gradient elution was employed as follows: 5 % A (0 ~ 2 min); 5 %~95 % A (2 ~ 42 min); 95 % A (42 ~ 47 min); 95 %~5% A (47 ~ 47.1 min); 5 % A (47.1 ~ 50 min).

MS data were collected using a Q-Orbitrap-MS with HESI-II (Thermo Fisher Scientific). MS's parameters were set as follows: RF lens amplitude (60), spray voltages (–2.5/+3.0 kV), vaporizer temperature (350 °C), capillary temperature (320 °C), sweep gas (0 arb), sheath gas (35 arb), and auxiliary gas (10 arb). We adopted the full mass/ddMS2 mode with the following parameter settings: stepped normalized collision energy (20/40/60 eV), resolution MS1 (70,000) and MS2 (17,500), automatic gain control target values MS1 ($1e^6$) and MS2 ($2e^5$), maximum injection time MS1 (100 ms) and MS2 (50 ms), and full scan range (*m/z* 100 to 1500). MS data of chemical components were analyzed using Thermo Fisher Scientific Xcalibur 4.1. The MS1 and MS2 fragments were compared with the mzVault database and literature data to identify chemical components, and the maximum relative mass error allowed was 10 ppm.

2.5. Cell culture

Kunming Cell Bank, Chinese Academy of Sciences (Kunming, China) provided the fetal lung fibroblast cells (MRC-5), murine fibroblast cells (L929), non-small cell lung cancer cells (NCI-H1299), and non-small cell lung adenocarcinoma cells (A549). All cell lines have been identified by STR (short tandem repeat) profiling. L929, NCI-H1299, and A549 cell lines were cultured in RPMI 1640 medium supplemented with 10 % FBS, 2 mM glutamine, 100 U/mL penicillin, and 100 μg/mL streptomycin. MRC-5 cells were maintained in DMEM with the same supplements. All cell lines were incubated at 37 °C with 5 % CO_2 in a humidified atmosphere.

2.6. Cytotoxic activity

MTT assay assessed the cytotoxic activity of *A. trifoliata* seed EE and WE against MRC-5, L929, NCI-H1299, and A549 cells with cisplatin as positive control. We dissolved *A. trifoliata* seed EE and WE in DMSO and serially diluted two times using culture medium (the ultimate concentration of DMSO < 0.05 %). Cell suspension (80 μL, 5×10^3 cells/well) was seeded into a 96-well plate. For the blank group, we added culture medium (80 μL). After 24 h of cultivation, different concentrations of *A. trifoliata* seed EE or WE solutions (20 μL) were added to the experimental group, with final concentrations of 10, 20, 40, 80, and 160 μg/mL. To the blank group and negative group, we added 20 μL of culture medium. After continuing to culture for 48 h, MTT solution (5 mg/mL) was added and incubated for 4 h. Afterward, the formazan crystals were dissolved by adding DMSO (150 μL/well), and the microplate reader (Thermo Fisher Scientific, Inc.) was used to measure the absorbance (Ab) at 490 nm. The following formula was applied to calculate the cell viability rate:

$$Cell\ viaibility\ rate = \left[\frac{Ab(experimental\ group) - Ab(blank\ group)}{Ab(negative\ group) - Ab(blank\ group)}\right] \times 100\%$$

2.7. Colony formation test

The antiproliferative action of *A. trifoliata* seed EE on the A549 cell line was assessed using the colony formation assay. A549 cells were digested, counted, seeded in a 6-well plate (200 cells per well), and cultured for 24 h. Subsequently, culture medium containing different concentrations of *A. trifoliata* seed EE (0, 30, 40, 50, 60, 70 μg/mL) was pipetted into the 6-well plate and continued to culture for 48 h. Afterward, we replaced the old medium with a fresh medium without *A. trifoliata* seed EE solution and incubated the cells for 7 d. The following staining process was performed: removing the culture medium, PBS wash twice, fixation for 30 min with formaldehyde solution (10 %, 700 μL), discarding the fixative, staining for 15 min with crystal violet solution (0.1 %, 700 μL), rinsing with water, and air drying for 24 h. The following formula was used to get the colony formation rate:

$$Clone\ formation\ rate = \frac{Colony\ number}{Inoculated\ cell\ number} \times 100\%$$

2.8. Cell cycle assay

The cell cycle was evaluated in compliance with the guidelines provided in the cell cycle staining kit (MultiSciences Biotech Co., Ltd., Hangzhou, China). In a 6-well plate, cells (4×10^5 cells/well) were inoculated and cultured for 24 h. Next, cells were exposed to various concentrations of *A. trifoliata* seed EE solution (0, 10, 20, 40, 60, and 80 μg/mL) for 48 h. After rinsing with PBS, 1 mL of DNA staining solution (containing 10 μL of permeabilization solution) was added and incubated in a dark environment for 30 min. The cell cycle was assayed using an ACEA NovoCyte™ flow cytometer (ACEA Biosciences, San Diego, CA, USA).

2.9. Cell apoptosis detection

2.9.1. Morphology observation

Morphological observations were conducted to determine the effect of *A. trifoliata* seed EE on A549 cell apoptosis. In a 6-well plate, A549 cells (4×10^5 cells per well) were incubated for 24 h and treated with a fresh medium that included various concentrations of *A. trifoliata* seed EE (0, 20, 40, 60, and 80 μg/mL) for 48 h. Finally, the Leica DMi8 microscope (Leica Microsystems, Germany) was used to observe the morphological changes of A549 cells.

2.9.2. AO/EB double staining assay

In the AO/EB double staining assay, the AO dye solution was obtained by adding 1 mg of AO to 10 mL of PBS and allowing it to dissolve entirely. An identical procedure was used to prepare the EB dye solution. The AO dye solution and EB dye solution were combined in equal ratios (1:1) to prepare the AO/EB solution. A549 cell line treatment was performed as described above. Then, we washed cells twice with PBS, added 1 mL of AO/EB solution (AO, 100 μg/mL; EB, 100 μg/mL), and stained the cells in the dark for 5 min. Finally, we observed the cells with a fluorescence microscope.

2.9.3. Hoechst 33,258 staining detection

Hoechst 33,258 staining was performed using the apoptosis Hoechst staining kit (Beyotime, Shanghai, China). Cells were handled in the same way as described above. After fixation for 10 min using 4 % paraformaldehyde solution (500 μL) and washing with PBS, cells were stained for 5 min in the dark using Hoechst 33,258 staining solution (500 μL). Eventually, a fluorescence microscope was used to examine nuclear morphology alterations.

2.9.4. Annexin V-PE/7-AAD double staining detection

The quantification of apoptosis in the A549 cell line was measured by Annexin V-PE/7-AAD double staining assay. According to the guidelines provided in Annexin V-PE/7-AAD apoptosis kit (MultiSciences Biotech Co., Ltd., Hangzhou, China), A549 cells were cultured for 24 h in a 6-well plate (4×10^5 cells per well) and treated with varied concentrations of *A. trifoliata* seed EE solutions (0, 10, 20, 40, 60, and 80 μg/mL) for 48 h. Cells were collected after washing with pre-cooled PBS and centrifuging, and 500 μL of 1 × binding buffer was applied to resuspend cells. Afterward, cells were stained for 5 min in the dark with 5 μL of Annexin V-PE and 10 μL of 7-AAD. Finally, flow cytometry was used to measure apoptosis rates.

2.10. JC-1 assay

JC-1 assay detected the effect of *A. trifoliata* seed EE on the mitochondrial membrane potential (ΔΨm). According to the guidelines of the JC-1 kit (Beyotime, Shanghai, China), A549 cells (4×10^5 cells per well) were cultured for 24 h in a 6-well plate and processed for 48 h with *A. trifoliata* seed EE at different concentrations (0, 10, 20, 40 μg/mL). After rinsing with PBS twice and incubation for 20 min in a mixture of fresh medium (900 μL) and JC-1 working solution (900 μL), the supernatant was removed, and JC-1 staining buffer was used to wash the cells twice. At the end, cells were viewed using an inverted fluorescence microscope.

2.11. Wound healing assay

Wound healing assays were done to assess the impact of *A. trifoliata* seed EE on the cell migratory capacity. *A. trifoliata* seed EE solutions of different concentrations (0, 2, 4, 8, and 10 μg/mL) were prepared using culture medium containing 0.5 % FBS. In a 6-well plate, A549 cells (5×10^5 cells per well) were cultured until the cells formed a confluent monolayer. After using a pipette tip (200 μL) to vertically scrape the cells, floating cells were removed by washing with PBS. Next, 2 mL of prepared *A. trifoliata* seed EE solution was added and incubated for 24 h. Eventually, a Leica DMi8 microscope was employed to record the wound width at 0 and 24 h. The migration rate (%) was used to assess the cell migration ability, which was calculated as follows:

$$Migration\ rate = \frac{Wound\ width(0\ h)\ - Wound\ width(24\ h)}{Wound\ width(0\ h)} \times 100\%$$

2.12. Transwell invasion detection

Transwell invasion assay was conducted using Corning® BioCoat™

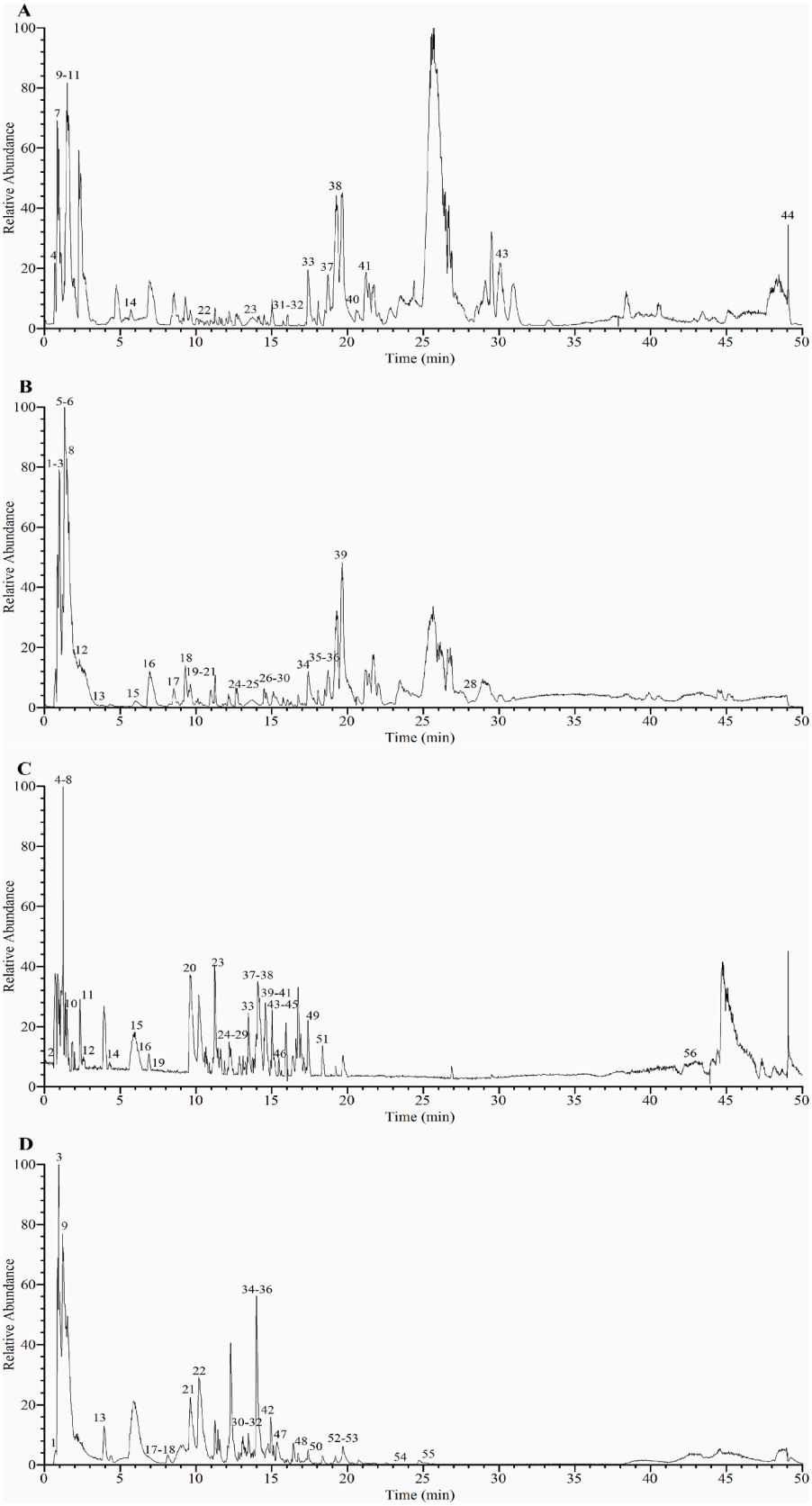

Fig. 1. UHPLC-Q-Orbitrap-MS base peak chromatograms of *A. trifoliata* seed EE and WE. **(A)** EE in positive ion mode; **(B)** EE in negative ion mode; **(C)** WE in positive ion mode; **(D)** WE in negative ion mode.

Table 1
Chemical composition of *A. trifoliata* seed EE and WE were authenticated using UHPLC-Q-Orbitrap-MS in positive and negative ion modes.

Peak NO.	RT [min] [a]	Identification [b]	Formula	$[M+H]^+$ (*m/z*)	$[M-H]^-$ (*m/z*)	Error ppm [c]	MS^2 fragmentions	EE [d]	WE [d]
1	0.846	Mannitol	$C_6H_{14}O_6$		181.07024	−8.4	163.05974, 101.02282, 89.02282, 71.01231, 59.01236	√	–
2	0.853	Lactose	$C_{12}H_{22}O_{11}$		387.11298 $[M+HCOO]^-$	−3.7	341.10754, 179.05484, 161.04402, 119.03336, 101.02274	√	–
3	0.912	Quinic acid	$C_7H_{12}O_6$		191.05467	−7.5	173.04398, 155.03276, 127.03851, 111.04359, 109.02777	√	–
4	0.951	Isocitric acid	$C_6H_8O_7$		191.01819	−8.0	173.00748, 154.99692, 129.01772, 111.00710, 87.00710	–	√
5	0.959	*γ*-Aminobutyric acid	$C_4H_9NO_2$	104.07061		0.0	87.04430, 86.06025, 69.03734, 60.08142, 58.06284	√	√
6	1.107	*D*-Glucaric acid	$C_6H_{10}O_8$		209.02893	−1.4	191.01833, 147.02786, 133.01270, 129.01781, 115.00211	√	–
7	1.181	Sucrose	$C_{12}H_{22}O_{11}$		341.10739	−0.4	179.05473, 161.04419, 119.03326, 113.02282, 101.02280	√	–
8	1.376	*L*-Tyrosine	$C_9H_{11}NO_3$	182.08069		−2.6	165.05396, 147.04341, 136.07521, 123.04376, 119.04890	√	√
9	1.384	Citric acid	$C_6H_8O_7$		191.01830	−7.5	173.00752, 129.01776, 111.00716, 87.00715, 85.02789	√	√
10	1.399	Nicotinic acid	$C_6H_5NO_2$	124.03899		−2.5	106.02927, 96.04453, 80.04984, 78.03418	√	–
11	1.414	Adenosine	$C_{10}H_{13}N_5O_4$	268.10312		−3.4	136.06134, 133.04875, 119.03503, 115.03862, 94.04015	√	–
12	1.436	Deoxyadenosine	$C_{10}H_{13}N_5O_3$	252.10811		−4.0	136.06133, 119.03489, 117.05437, 99.04405, 94.04004	–	√
13	1.471	Guanosine	$C_{10}H_{13}N_5O_5$	284.09778		−4.1	152.05605, 135.02959, 110.03466, 109.05067	–	√
14	1.479	Guanine	$C_5H_5N_5O$	152.05615		−3.5	135.02954, 110.03471, 109.05070, 82.03996	–	√
15	1.532	*L*-Leucine	$C_6H_{13}NO_2$	132.10152		−2.9	115.07529, 86.09676, 69.07037	√	√
16	2.280	1-Methyladenosine	$C_{11}H_{15}N_5O_4$	282.11871		−3.4	150.07690, 136.06105, 133.04935	–	√
17	2.382	*L*-Phenylalanine	$C_9H_{11}NO_2$		164.07021	−9.1	147.04362, 120.05192, 103.05370, 91.05366, 72.00755	√	√
18	3.780	Protocatechuic acid	$C_7H_6O_4$		153.01784	−9.8	153.01781, 109.02791, 108.02007, 91.01744	√	–
19	3.784	Gentisic acid	$C_7H_6O_4$		153.01773	−9.5	109.02785, 108.02001, 91.01729	–	√
20	4.201	5-Hydroxymethylfurfural	$C_6H_6O_3$	127.03861		−2.8	109.02824, 99.04404, 97.02848, 81.03376	–	√
21	5.702	Adenine	$C_5H_5N_5$	136.06139		−2.8	119.03500, 109.01053, 94.04016, 92.02438, 67.02952	√	√
22	6.013	Protocatechualdehyde	$C_7H_6O_3$		137.02284	−9.7	119.01231, 109.02791, 108.02001, 93.03304	√	√
23	6.588	Higenamine	$C_{16}H_{17}NO_3$	272.12704		−4.0	255.10028, 237.08990, 161.05899, 143.04855, 123.04372	–	√
24	7.540	Esculin	$C_{15}H_{16}O_9$		339.07074	−4.2	177.01779, 149.02274, 133.02785	–	√
25	7.585	2-Isopropylmalic acid	$C_7H_{12}O_5$		175.05978	−8.1	157.04990, 115.03846, 113.05920, 85.06428	√	√
26	7.880	Orsellinic acid	$C_8H_8O_4$	169.04884		−4.1	151.03836, 141.05406, 126.03071, 125.02290, 109.02831	–	√
27	8.595	Procyanidin B1	$C_{30}H_{26}O_{12}$		577.13293	−3.8	451.10236, 425.08661, 407.07535, 289.07056, 125.02283	√	–
28	9.023	(+)-Catechin hydrate	$C_{15}H_{14}O_6$		289.07086 $[M-H_2O-H]^-$	−3.1	245.08104, 227.06885, 205.04938, 203.07007, 151.03854	√	–
29	9.532	1-Caffeoylquinic acid	$C_{16}H_{18}O_9$		353.08661	−3.4	191.05473, 179.03391, 161.02286, 135.04352, 127.03864	√	√
30	9.630	7-Hydroxycoumarin	$C_9H_6O_3$	163.03828		−4.2	145.02780, 135.04353, 117.03325, 107.04904, 89.03879	–	√
31	9.795	Leucinic acid	$C_6H_{12}O_3$		131.06979	−9.8	113.02259, 102.98717, 85.06430, 69.03302	√	–
32	9.850	Caffeic acid	$C_9H_8O_4$		179.03340	−8.8	161.04430, 135.04356, 134.03571, 117.01770, 107.04860	–	–
33	10.084	Cryptochlorogenic acid	$C_{16}H_{18}O_9$		353.08649	−3.7	191.05463, 179.03345, 173.04407, 137.02292, 111.04372	√	√
34	10.626	13-*α*-(21)-Epoxyeurycomanone	$C_{20}H_{24}O_{10}$	425.14032		−9.2	407.17905, 389.16882, 371.15869, 341.14795, 263.13785	√	–
35	11.458	Vanillin	$C_8H_8O_3$	153.05405		−3.7	125.05932, 111.04397, 93.03365, 65.03914	–	√
36	12.208	7-Methoxycoumarin	$C_{10}H_8O_3$	177.05411		−2.9	162.03027, 149.05904, 145.02783, 134.03568, 117.03328	–	√
37	12.371	5-Hydroxy-1-tetralone	$C_{10}H_{10}O_2$	163.07463		−4.5	145.02780, 135.04355, 117.03326, 103.05421, 93.07001	–	√
38	12.486	3,5-Dimethoxy-4-hydroxybenzalde	$C_9H_{10}O_4$	183.06453		−3.6	155.06952, 140.04614, 123.04379, 95.04933	–	√

(*continued on next page*)

Table 1 (*continued*)

Peak NO.	RT [min] [a]	Identification [b]	Formula	$[M+H]^+$ (*m/z*)	$[M-H]^-$ (*m/z*)	Error ppm [c]	MS^2 fragmentions	EE [d]	WE [d]
39	13.191	Skimmin	$C_{15}H_{16}O_8$	325.09042		−4.2	307.07986, 181.04871, 163.03827, 145.02783, 117.03324	–	√
40	13.262	Vitexin rhamnoside	$C_{27}H_{30}O_{14}$	579.16827		−4.4	433.11102, 313.06915, 283.05884, 271.05829, 165.01707	–	√
41	13.291	Rutin	$C_{27}H_{30}O_{16}$		609.14404	−3.4	301.03421, 300.02631, 271.02368, 255.02875, 151.00211	–	√
42	13.464	Camelliaside B	$C_{32}H_{38}O_{19}$		725.19122	−3.1	327.05112, 285.03928, 284.03149, 163.00195, 151.00217	–	√
43	13.598	Morin	$C_{15}H_{10}O_7$	303.04883		−3.6	285.22012, 257.04349, 229.04854, 165.01761, 153.01767	√	√
44	13.606	Hyperoside	$C_{21}H_{20}O_{12}$		463.08661	−3.4	301.03415, 300.02640, 271.02377, 243.02864, 227.03362	√	√
45	13.887	Calceolarioside B	$C_{23}H_{26}O_{11}$		477.13846	−3.7	315.10739, 227.09114, 221.04434, 179.03334, 161.02287	√	√
46	14.067	Poncirin	$C_{28}H_{34}O_{14}$		593.18561	−3.3	327.04938, 285.03922, 284.03146, 255.02866, 227.03363	–	√
47	14.300	Kaempferol-3-*O*-rutinoside	$C_{27}H_{30}O_{15}$		593.14886	−3.9	327.04904, 285.03925, 284.03146, 255.02867, 227.03368	–	√
48	14.431	Narcissoside	$C_{28}H_{32}O_{16}$	625.17346		−4.6	315.04980, 314.04211, 299.01846, 271.02368, 243.02866	–	√
49	14.436	Isosakuranin	$C_{22}H_{24}O_{10}$	449.13983		−9.8	287.05371, 258.05029, 241.04774, 177.09023, 153.01753	–	√
50	14.538	Isochlorogenic acid B	$C_{25}H_{24}O_{12}$		515.11749	−3.9	353.06840, 191.05461, 179.03345, 173.04401, 135.04352	√	√
51	14.576	Camphor	$C_{10}H_{16}O$	153.12680		−3.9	135.11621, 107.08543, 93.06999, 81.07019, 69.07028	–	√
52	14.607	Quercitrin	$C_{21}H_{20}O_{11}$		447.09174	−3.5	301.03421, 300.02652, 285.03922, 227.03369, 151.00220	√	–
53	14.670	Astragalin	$C_{21}H_{20}O_{11}$	449.10599		−4.1	287.05365, 165.01735, 153.01759, 121.02808	–	√
54	14.922	Azelaic acid	$C_9H_{16}O_4$		187.09613	−7.8	169.08569, 143.10609, 125.09562, 97.06426	√	–
55	14.923	Isorhamnetin	$C_{16}H_{12}O_7$	317.06424		−4.2	302.04059, 285.03781, 257.04303, 153.01751, 121.02818	–	√
56	15.033	Diosmin	$C_{28}H_{32}O_{15}$	609.17871		−4.4	463.12073, 301.06927, 286.04578, 258.05109, 153.01793	–	√
57	15.054	Rosarin	$C_{20}H_{28}O_{10}$		427.15924	−4.1	179.05421, 161.04445, 149.04417, 119.03340, 101.02280	√	–
58	15.13	Isochlorogenic acid C	$C_{25}H_{24}O_{12}$		515.11761	−3.7	353.08643, 191.05470, 179.03349, 173.04408, 135.04356	√	–
59	15.143	Coumarin	$C_9H_6O_2$	147.04350		−3.8	147.04352, 119.04887, 105.06959, 103.05427, 91.05441	–	√
60	15.192	Rosavin	$C_{20}H_{28}O_{10}$		427.15924	−4.1	191.05491, 179.05476, 161.04373, 119.03345, 101.02277	–	√
61	15.750	Kaempferol	$C_{15}H_{10}O_6$	287.05405		−3.4	269.04379, 259.05936, 165.01762, 153.01761, 121.02811	√	√
62	16.305	Limonin	$C_{26}H_{30}O_8$	471.19702		−9.2	453.33572, 425.34003, 407.32938, 395.32939, 111.08035	√	–
63	16.998	Forsythin	$C_{27}H_{34}O_{11}$		579.20599 $[M+HCOO]^-$	−4.0	371.14856, 356.12479, 218.38524, 161.04344, 121.02779	–	√
64	17.009	Arglabin	$C_{15}H_{18}O_3$	247.13185		−4.1	229.12120, 211.11087, 201.12654, 187.11093, 173.13181	–	√
65	17.392	*α*-Hederin	$C_{41}H_{66}O_{12}$	751.45911		−4.8	455.35382, 437.33936, 409.34659, 391.33499, 215.17882	√	–
66	17.432	Atractyloside A	$C_{21}H_{36}O_{10}$		493.22693 $[M+HCOO]^-$	−4.3	315.18036, 179.03387, 161.02287, 101.02280, 71.01228	–	√
67	17.448	Quercetin	$C_{15}H_{10}O_7$		301.03415	−4.1	273.03967, 257.04459, 245.04427, 229.04955, 151.00215	√	√
68	18.300	Macranthoidin B	$C_{65}H_{106}O_{32}$		1397.65283	−4.7	1351.64478, 881.48700, 749.44464, 601.19623, 585.37811	√	–
69	18.571	Jujuboside A	$C_{58}H_{94}O_{26}$		1251.59583 $[M+HCOO]^{-}$	−4.6	1085.55029, 777.44238, 735.43036, 603.38782, 585.37622	√	–
70	18.709	Oleanonic acid	$C_{30}H_{46}O_3$	455.35043		−3.4	409.34521, 391.33344, 249.18433, 177.16319, 119.08531	√	–
71	19.430	Pedunculoside	$C_{36}H_{58}O_{10}$		695.39825 $[M+HCOO]^-$	−4.2	487.34091, 356.12576, 247.01979, 179.03331, 161.02277	–	√
72	19.487	Asiaticoside	$C_{48}H_{78}O_{19}$		957.50281	−3.8	649.39539, 631.38696, 487.34079, 455.31494, 245.06425	–	√
73	19.621	Ursonic acid	$C_{30}H_{46}O_3$	455.35065		−2.9	437.33987, 425.34036, 409.34558, 249.18417, 207.17366	√	–
74	19.630	Asperosaponin VI	$C_{47}H_{76}O_{18}$		973.49915 $[M+HCOO]^-$	−2.3	603.38824, 323.09705, 263.07666, 221.06546, 179.05481	√	–
75	20.303	Prunetin	$C_{16}H_{12}O_5$	285.0752		−1.9	267.20944, 241.19490, 225.16264, 211.14728, 107.08553	√	–

(*continued on next page*)

Table 1 (*continued*)

Peak NO.	RT [min] [a]	Identification [b]	Formula	$[M+H]^+$ (*m/z*)	$[M-H]^-$ (*m/z*)	Error ppm [c]	MS^2 fragmentions	EE [d]	WE [d]
76	21.914	Glabrolide	$C_{30}H_{44}O_4$	469.32974		−3.2	451.31940, 439.31888, 423.32574, 405.31265, 189.16304	√	√
77	23.827	Medicagenic acid	$C_{30}H_{46}O_6$		501.32050	−3.3	483.31131, 457.33151, 439.32056, 381.31616, 365.28317	–	√
78	25.135	Bayogenin	$C_{30}H_{48}O_5$		487.34106	−3.8	421.30841, 409.30759, 393.31641, 391.29700, 363.26688	–	√
79	28.360	Methyl hexadecanoate	$C_{17}H_{34}O_2$		315.25287 $[M+HCOO]^-$	−3.8	313.23734, 297.24240, 269.24683, 171.13747, 127.11124	√	–
80	30.101	*α*-Linolenic acid	$C_{18}H_{30}O_2$	279.23077		−3.9	261.22058, 243.20938, 123.11652, 109.10110, 95.08569	√	–
81	42.188	Vitamin D3	$C_{27}H_{44}O$	385.34470		−4.7	367.33514, 241.19362, 213.16374, 123.08012, 109.06468	–	√
82	49.860	Vitamin D2	$C_{28}H_{44}O$	397.34488		−4.1	315.30273, 287.27295, 257.22592, 161.13177, 147.11618	√	–

[a]RT: Retention time. [b] Identification: Phytochemical compounds were identified by comparing the MS1 and MS2 fragments with the data in the mzVault database and references. In addition, the detailed analysis of fragmentation patterns is presented in the Supplementary Material. [c] Error ppm represents mass error in parts per million (ppm) and was obtained from Thermo Fisher Scientific Xcalibur 4.1 software. [d] "√" means detected from extracts, "-" means undetected from extracts.

Matrigel® invasion chambers (Corning, New York, USA). Firstly, 750 μL of *A. trifoliata* seed EE solutions (0, 10, 15, 20, 25, and 30 μg/mL) prepared using 15 % FBS medium were added to the lower chamber. In the upper chamber, 250 μL of A549 cell suspension (1×10^5 cells per well) in 5 % FBS medium and 250 μL of *A. trifoliata* seed EE solution prepared with 5 % FBS medium were added (the final concentration of *A. trifoliata* seed EE was the same as that in the lower chamber). After 48 h of incubation, 4 % paraformaldehyde was applied to fix the cells for 2 min. Afterward, cells were incubated for 20 min with anhydrous methanol and stained for 15 min with 0.1 % crystal violet. After rinsing twice with PBS, images were captured using a Leica DMi8 microscope, and the number of invaded cells was counted using Image J software.

2.13. Western blotting analysis

In a 6-well plate, A549 cells (4×10^5 cells per well) were cultured for 24 h and were treated for 48 h with 0 and 80 μg/mL *A. trifoliata* seed EE solutions (2 mL). Next, RIPA lysis buffer was employed to extract the total protein, and BCA protein assay kits were utilized to detect the total protein concentration. Afterward, extracted proteins were separated by 10 %-15 % SDS-PAGE, and the separated proteins were transferred to PVDF membranes by wet transfer method (constant voltage 220 V, 60 min). TBS-T (TBS, 0.1 % Tween-20) containing 5 % skimmed milk powder was used to block the PVDF membranes for 1 h, after which the PVDF membranes were placed inside the primary antibody solution and

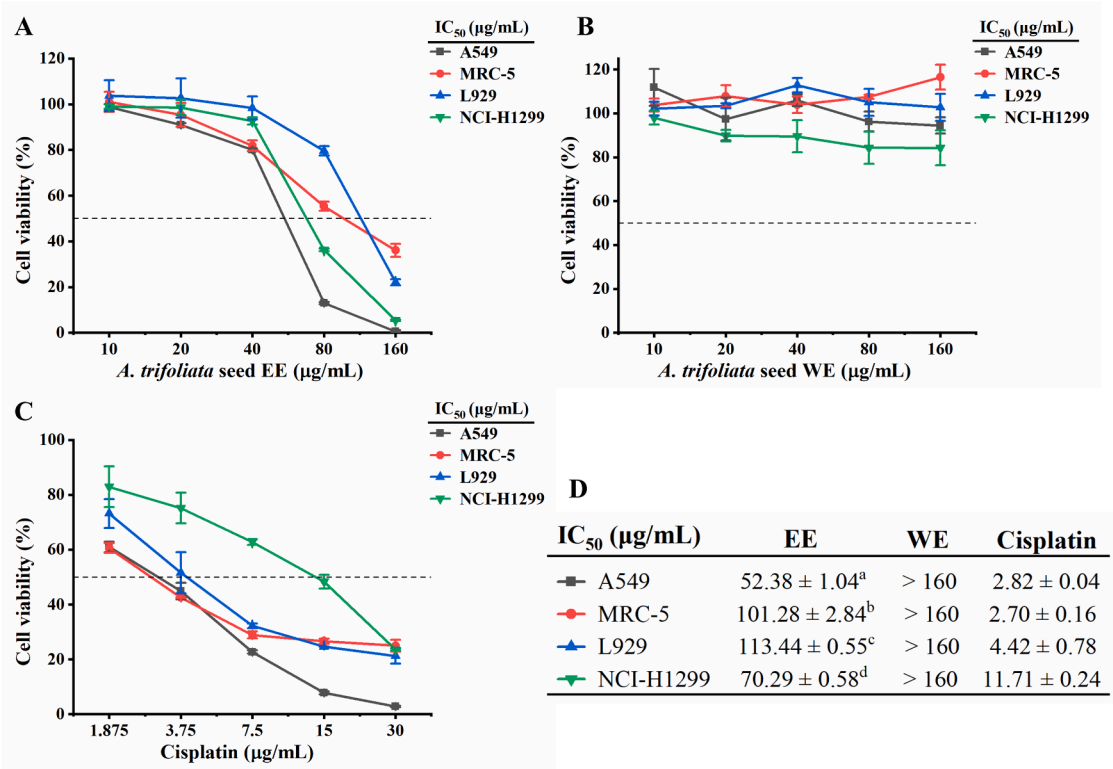

Fig. 2. Cytotoxicity of *A. trifoliata* seed EE and WE. **(A, B)** Cytotoxic activity of *A. trifoliata* seed EE and WE against A549, MRC-5, L929, and NCI-H1299 cell lines. **(C)** Cytotoxic activity of cisplatin against A549, MRC-5, L929, and NCI-H1299 cell lines. **(D)** IC_{50} values of *A. trifoliata* seed EE and WE and positive control drug cisplatin. IC_{50}: Half-inhibitory concentration. Data were expressed as means ± standard deviation (SD). Each data point represents mean values, and error bars represent SD. Differences between groups were determined by one-way analysis of variance (ANOVA) with the least significant difference (LSD). Different letters in the same column (a-d) represent significant differences ($p < 0.05$).

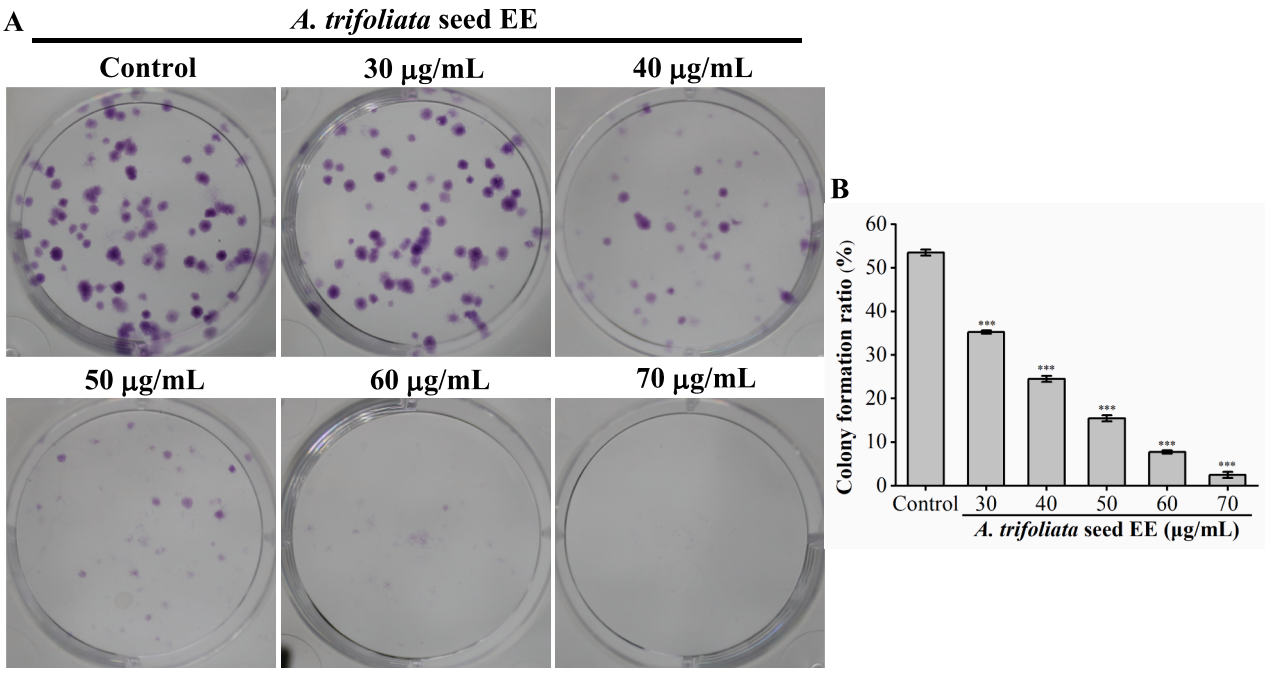

Fig. 3. *A. trifoliata seed* EE blocked A549 cells' colony formation. **(A)** Representative images of colony formation. **(B)** The colony formation rates (%) of A549 cells. Data were presented as means ± SD. Bars represent mean values, and error bars represent SD. Statistical significance was determined by one-way analysis of variance (ANOVA) with LSD (***$p < 0.001$ vs the control group).

incubated at 4 °C overnight. After three washes with TBST (5 min each) and blotting for 1 h with secondary antibodies, protein bands were detected using ChemiDoc touch imaging system with super ECL detection reagent and quantified by Image Lab software (Bio-Rad Laboratories, Inc., Hercules, CA, USA).

2.14. Statistical analysis

The data in this study are expressed as means ± standard deviation (SD). SPSS 26.0 software (SPSS, Inc., Chicago, IL, USA) was used for statistical analysis. Significant differences between the two groups were evaluated using the two-tailed unpaired *t*-test, and multiple different groups were compared by one-way analysis of variance (ANOVA) with the least significant difference (LSD). The *p*-values < 0.05 were considered statistically significant (*$p < 0.05$, **$p < 0.01$, ***$p < 0.001$).

3. Results

3.1. Phytochemicals of A. trifoliata seed EE and WE

The extraction rates of *A. trifoliata* seed EE and WE were 3.64 % and 4.68 %, respectively. The phytochemical constituents of EE and WE were analyzed by UHPLC-Q-Orbitrap-MS in positive and negative ion modes. As shown in Fig. 1 and Table 1, a total of 82 compounds were identified by analyzing the MS1 and MS2 fragments of chemical components in *A. trifoliata* seed EE and WE and comparing them with the data in the mzVault database and references (detailed analysis of fragmentation patterns in Supplementary Material), of which 44 were identified in EE and 56 in WE, including 18 flavonoids, 15 terpenoid compounds, 17 phenol compounds, and 32 other types of constituents. Eighteen identified flavonoid compounds were procyanidin B1 (27), (+)-catechin hydrate (28), vitexin rhamnoside (40), rutin (41), camelliaside B (42), morin (43), hyperoside (44), poncirin (46), kaempferol-3-*O*-rutinoside (47), narcissoside (48), isosakuranin (49), quercitrin (52), astragalin (53), isorhamnetin (55), diosmin (56), kaempferol (61), quercetin (67), and prunetin (75). Seventeen identified phenol compounds were *L*-tyrosine (8), protocatechuic acid (18), gentisic acid (19), protocatechualdehyde (22), higenamine (23), esculin (24), orsellinic acid (26), 1-caffeoylquinic acid (29), 7-hydroxycoumarin (30), caffeic acid (32), cryptochlorogenic acid (33), vanillin (35), 5-hydroxy-1-tetralone (37), 3,5-dimethoxy-4-hydroxybenzaldehyde (38), calceolarioside B (45), isochlorogenic acid B (50), and isochlorogenic acid C (58). Fifteen identified terpenoid compounds were camphor (51), limonin (62), arglabin (64), α-hederin (65), atractyloside A (66), macranthoidin B (68), jujuboside A (69), oleanonic acid (70), pedunculoside (71), asiaticoside (72), ursonic acid (73), asperosaponin VI (74), glabrolide (76), medicagenic acid (77), and bayogenin (78). Based on past research on the phytochemical components of *A. trifoliata* seed (Lei et al., 2015; Su et al., 2021; Chen et al., 2022), apart from *L*-tyrosine (8), *L*-teucine (15), *L*-phenylalanine (17), leucinic acid (31), α-linolenic acid (80), esculin (24), 2-isopropylmalic acid (25), procyanidin B1 (27), caffeic acid (32), skimmin (39), rutin (41), hyperoside (44), calceolarioside B (45), astragalin (53), isorhamnetin (55), coumarin (59), kaempferol (61), quercetin (67), and medicagenic acid (77), the remaining 63 compounds were identified in *A. trifoliata* seed for the first time. Based on the above data, *A. trifoliata* seed EE and WE were rich in flavonoids, phenols, and terpenoids.

3.2. Cytotoxicity of A. trifoliata seed EE and WE

Cytotoxic activity of *A. trifoliata* seed EE and WE was evaluated by MTT assay against non-cancer cell lines (MRC-5 and L929) and cancer cell lines (NCI-H1299 and A549) with cisplatin as a positive control (Fig. 2). *A. trifoliata* seed EE displayed high cytotoxicity against cancer cells A549 (IC_{50}: 52.38 ± 1.04 μg/mL) and NCI-H1299 (IC_{50}: 70.29 ± 0.58 μg/mL), whereas exhibited low cytotoxicity against non-cancer cells L929 (IC_{50}: 113.44 ± 0.55 μg/mL) and MRC-5 (IC_{50}: 101.28 ± 2.84 μg/mL). Meanwhile, *A. trifoliata* seed WE showed insignificant cytotoxicity against cancer and non-cancer cells A549, NCI-H1299, MRC-5, and L929 (IC_{50}: > 160 μg/mL). These findings suggested that *A. trifoliata* seed EE exhibited selective cytotoxic activity on cancer cells, especially A549 cells. Therefore, *A. trifoliata* seed EE was selected for further investigation on its anticancer effects on A549 cells.

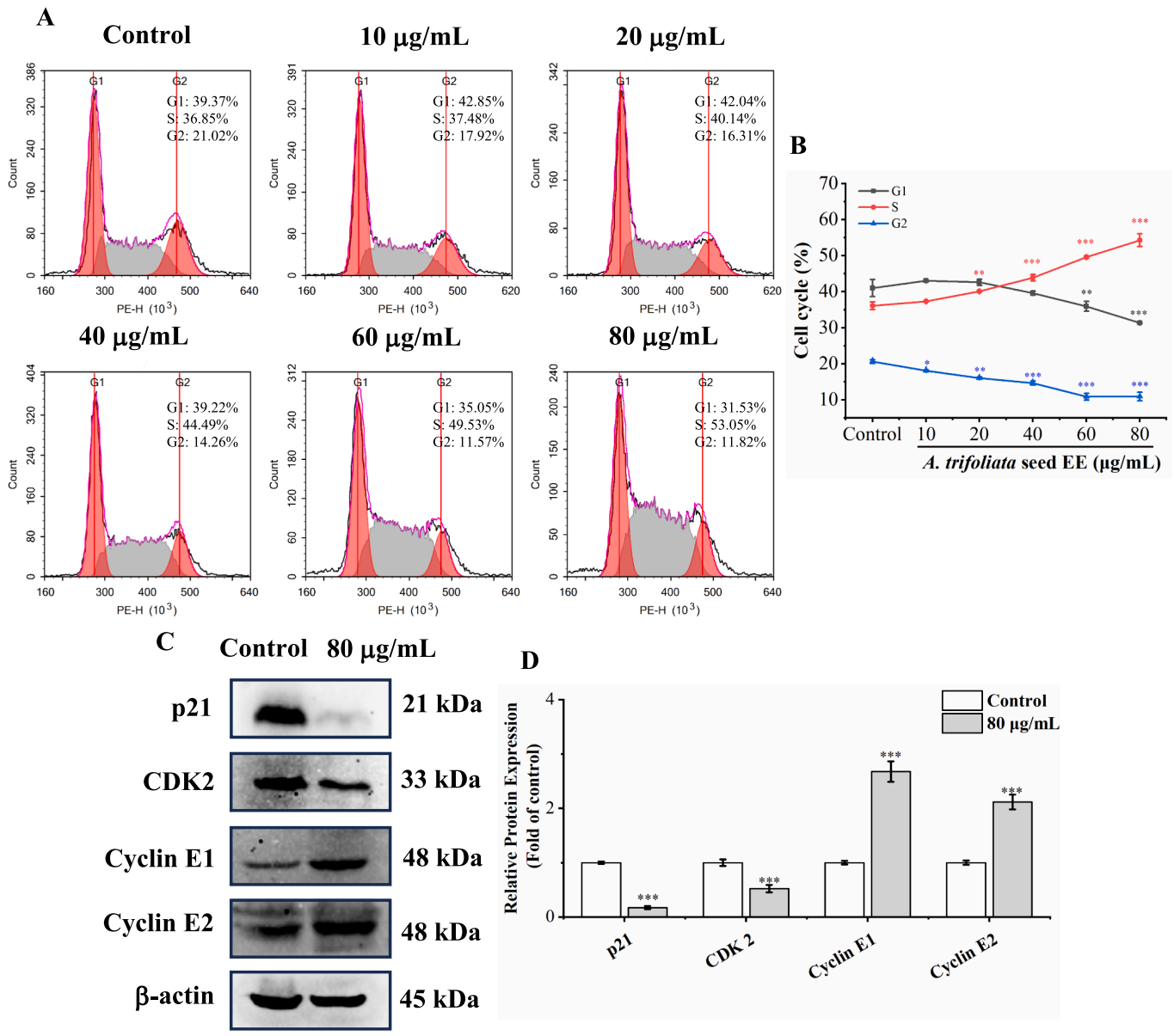

Fig. 4. *A. trifoliata* seed EE induced S phase arrest. **(A, B)** After treatment with *A. trifoliata* seed EE, cell cycle distribution was assayed by flow cytometry using the cell cycle staining kit. **(C, D)** Cell cycle-related proteins in *A. trifoliata* seed EE-treated cells were detected by western blotting. Data were expressed as means ± SD. Data points and histograms show mean values, and error bars represent SD. Statistical differences in cell cycle assay were detected using one-way analysis of variance (ANOVA) and LSD. Statistical differences in western blot analysis results were determined using the two-tailed unpaired *t*-test. * $p < 0.05$, ** $p < 0.01$, *** $p < 0.001$ versus the control group.

3.3. *A. trifoliata seed EE inhibited A549 cell proliferation*

The colony formation assay was utilized to investigate the effect of *A. trifoliata* seed EE on A549 cell proliferation. As illustrated in Fig. 3A and B, the number and size of A549 cell colonies were substantially lowered after *A. trifoliata* seed EE treatment. The colony formation rates of A549 cells treated with several doses of *A. trifoliata* seed EE (30, 40, 50, 60, and 70 μg/mL) were markedly lowered to 35.25 ± 0.35 %, 24.50 ± 0.70 %, 15.50 ± 0.70 %, 7.75 ± 0.35 %, and 2.50 ± 0.70 %, respectively, in comparison to the control group (53.50 ± 0.70 %). Hence, *A. trifoliata* seed EE exhibited concentration-dependent inhibition on A549 cell proliferation.

3.4. *A. trifoliata seed EE induced S phase arrest*

Cell cycle disorder leads to uncontrolled malignant proliferation of cancer cells (Chen et al., 2021a). To ascertain whether the anti-proliferative activity of *A. trifoliata* seed EE was triggered by cell cycle arrest, we examined the cell cycle distribution using flow cytometry (Fig. 4A and B). Aftertreatment with *A. trifoliata* seed EE at concentrations of 10, 20, 40, 60, and 80 μg/mL, S phase cell proportions were increased from 36.09 ± 1.07 % in control to 37.34 ± 0.19 %, 40.08 ± 0.08 %, 43.87 ± 0.87 %, 49.61 ± 0.31 %, and 54.31 ± 1.78 %, respectively. The results showed that *A. trifoliata* seed EE induced S cell cycle arrest and thus inhibited the A549 cell proliferation.

We used western blot analysis to examine S phase-regulatory protein levels in order to uncover the underlying mechanisms of *A. trifoliata* seed EE-induced suppression of the A549 cell cycle (Fig. 4C and D). *A. trifoliata* seed EE significantly down-regulated CDK2 and p21 and up-regulated cyclin E1 and cyclin E2 expression. Thus, *A. trifoliata* seed EE induced S cell cycle arrest by up-regulating cyclin E1 and cyclin E2 and down-regulating p21 and CDK2.

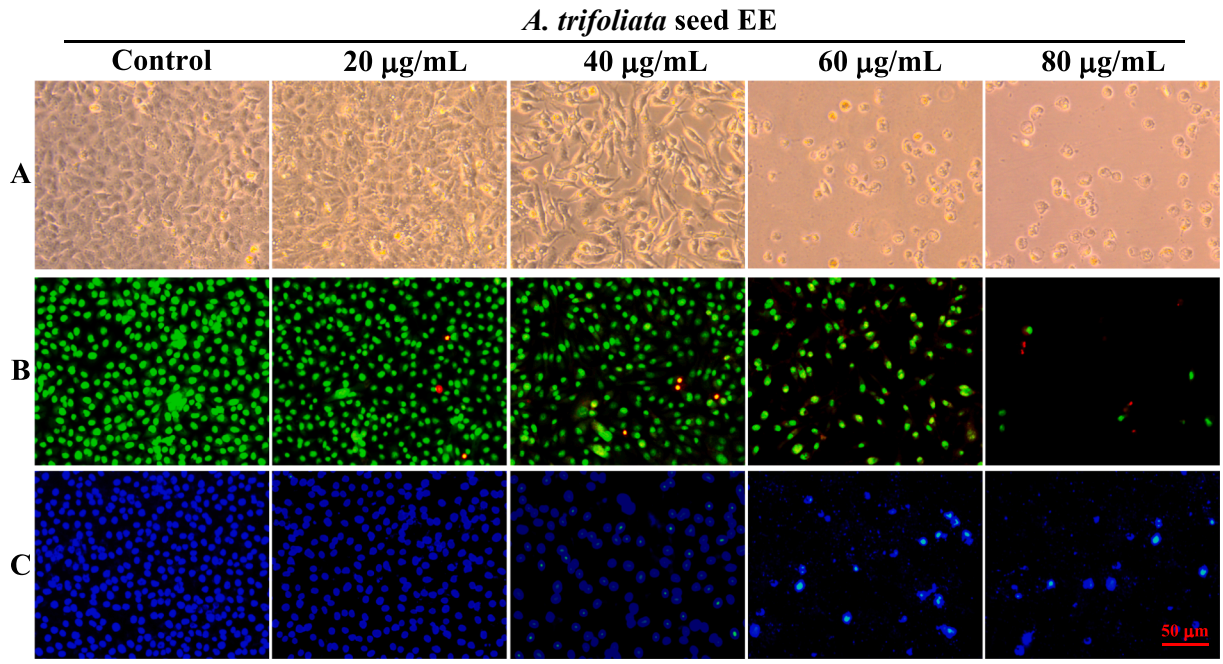

Fig. 5. Cell morphological and nuclear morphology changes in *A. trifoliata* seed EE-treated A549 cells. **(A)** Under a phase contrast microscope, cell morphological alterations of A549 cells were observed and recorded. **(B, C)** A549 cells were stained with AO/EB (B) and Hoechst 33,258 (C) and observed under an inverted fluorescence microscope to analyze nuclear morphological changes.

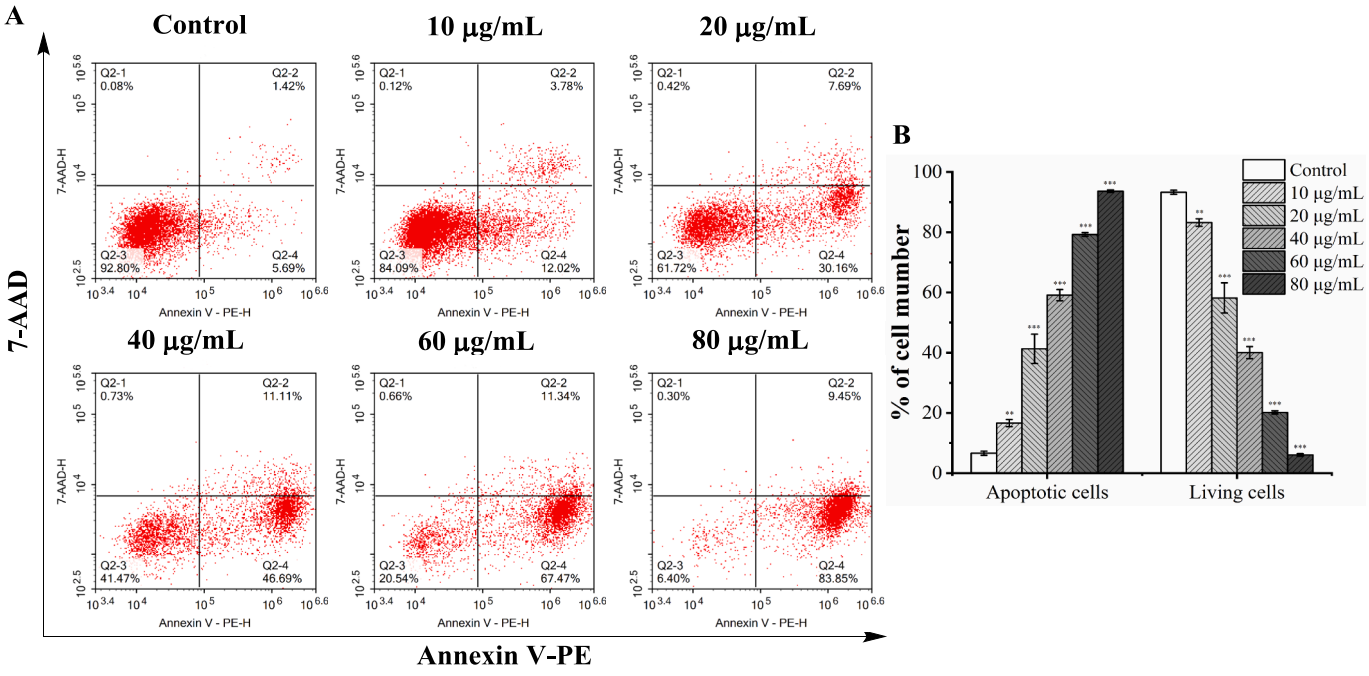

Fig. 6. *A. trifoliata* seed EE induced A549 cell apoptosis. **(A)** A549 cell apoptosis was detected by flow cytometry using Annexin V-PE/7-AAD staining. Early apoptotic cells in the lower right quadrant (PE+/7-AAD–); late apoptotic cells in the upper right quadrant (PE+/7-AAD+); living cells in the lower left quadrant (PE–/7-AAD–); necrotic cells in the upper left quadrant (PE–/7-AAD+). **(B)** The proportion of apoptotic and living cells. Data were expressed as means ± SD. Bars represent mean values, and error bars represent SD. Statistical significance was determined by one-way analysis of variance (ANOVA) with the LSD. Compared with the control group, $^{**}p < 0.01$, $^{***}p < 0.001$.

3.5. A. trifoliata seed EE induced apoptosis of A549 cells

Apoptosis induction has been recognized as a key tactic in tumor treatment (Yu et al., 2022). Morphological observations revealed that A549 cells treated with *A. trifoliata* seed EE exhibited morphological alterations of apoptosis, like cell rounding and shrinkage (Fig. 5A). Furthermore, to investigate further the nuclear morphology changes induced by *A. trifoliata* seed EE, AO/EB staining and Hoechst 33,258 staining were applied. In the AO/EB double staining assay (Fig. 5B), as *A. trifoliata* seed EE concentration raised, the proportion of apoptotic cells with orange-red fluorescent nuclei increased. In contrast, the cell proportion with green fluorescent nuclei decreased. As shown in Fig. 5C,

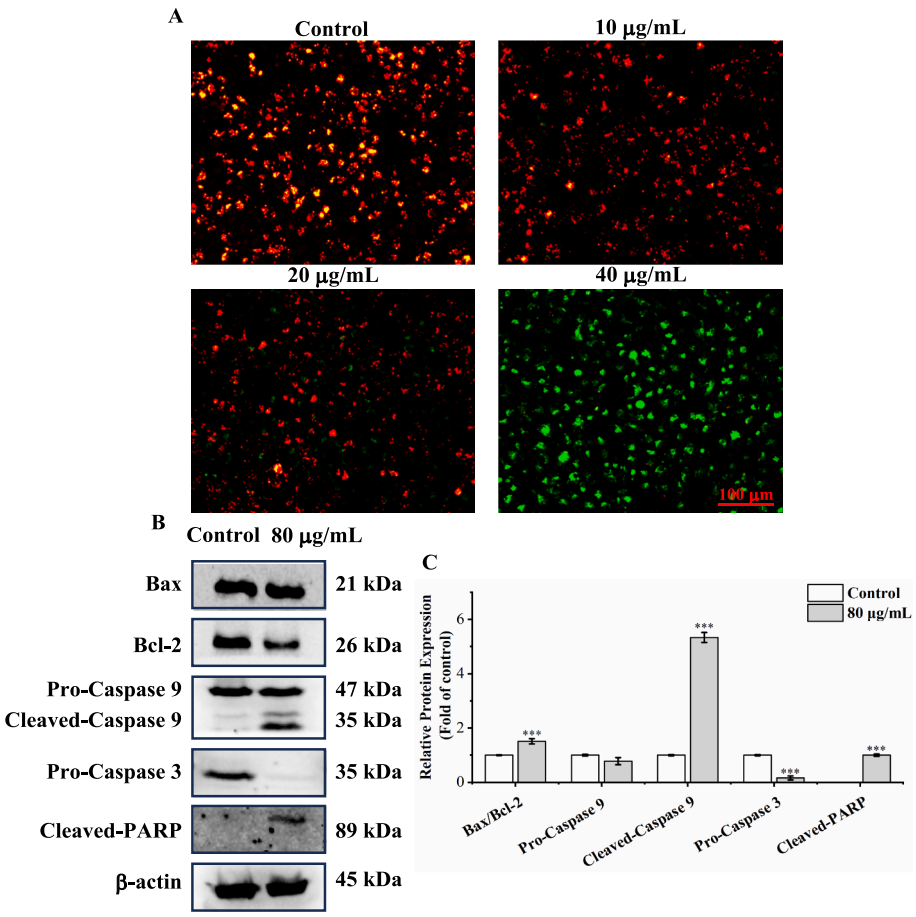

Fig. 7. *A. trifoliata* seed EE induced A549 apoptosis through the mitochondrial pathway. **(A)** Representative images of *A. trifoliata* seed EE-treated A549 cells stained with JC-1 probe. **(B, C)** Mitochondrial apoptosis pathway-related proteins in *A. trifoliata* seed EE-treated cells were detected by western blotting. Results are shown as means ± SD. Bars represent mean values, and error bars represent SD. Statistical differences were determined using the two-tailed unpaired *t*-test (***$p < 0.001$ versus the control group).

after being treated with *A. trifoliata* seed EE and staining with Hoechst 33258, the proportion of apoptotic cells with bright blue fluorescence and dense nuclei gradually increased.

The flow cytometry quantified the apoptosis induced by *A. trifoliata* seed EE utilizing Annexin V-PE/7-AAD staining (Fig. 6A and B). In contrast to the control group (6.62 ± 0.69 %), the ratio of A549 apoptotic cells treated with *A. trifoliata* seed EE (10, 20, 40, 60, and 80 μg/mL) increased significantly to 16.63 ± 1.18 %, 41.28 ± 4.85 %, 59.13 ± 1.88 %, 79.24 ± 0.61 % and 93.61 ± 0.43 %, respectively. Therefore, *A. trifoliata* seed EE induced A549 cell apoptosis in a concentration-dependent manner.

3.6. *A. trifoliata seed EE triggered apoptosis through the mitochondrial pathway*

Loss of mitochondrial membrane potential (ΔΨm) is a critical event during early apoptosis (Sivandzade et al., 2019). Hence, the fluorescent probe JC-1 was employed to assess mitochondrial membrane potential. After staining with JC-1 dye, in normal cells with high ΔΨm, JC-1 accumulates to form aggregates, emitting red fluorescence. In addition, in apoptotic cells with low ΔΨm, JC-1 is present as monomers, emitting green fluorescence. As illustrated in Fig. 7A, after treating with *A. trifoliata* seed EE, the proportion of green fluorescent cells gradually increased, and the percentage of red fluorescent cells gradually decreased. Particularly, after treatment with *A. trifoliata* seed EE at the dose of 40 μg/mL, A459 cells nearly completely showed green fluorescence. The aforementioned data demonstrated that *A. trifoliata* seed EE induced apoptosis by reducing ΔΨm in the A549 cell line.

Western blot assay was used to detect proteins associated with the mitochondrial apoptosis pathway (Fig. 7B and C). *A. trifoliata* seed EE lowered the expression of Bcl-2, while Bax expression was unchanged prominently. The Bax/Bcl-2 ratio exhibited significant up-regulation. Meanwhile, *A. trifoliata* seed EE markedly lowered pro-caspase 3 levels and enhanced the expression of cleaved-caspase 9 and cleaved-PARP. The above findings suggested that *A. trifoliata* seed EE activated the mitochondrial apoptotic pathway in the A549 cell line, which increased Bax/Bcl-2 ratio, activated caspase 9 and caspase 3, and caused PARP cleavage.

3.7. *A. trifoliata seed EE inhibited the migratory and invasive abilities of A549 cells*

Cancer metastasis is the leading cause of cancer death (Darzi et al., 2021). The effects of *A. trifoliata* seed EE on A549 cell migratory and invasive capacities were investigated using wound healing and transwell invasion assay. The wound healing assay results (Fig. 8A and B) indicated that compared with the control group (84.98 ± 3.72 %), the migration ratios of *A. trifoliata* seed EE-treated A549 cells (2, 4, 8, and 10 μg/mL) were remarkably decreased to 71.34 ± 1.85 %, 60.49 ± 1.17 %, 50.42 ± 2.46 %, and 45.09 ± 1.16 %, respectively. In addition, compared with the control group (1037.00 ± 18.38 cells per field), *A. trifoliata* seed EE (10, 15, 20, 25, and 30 μg/mL) significantly reduced the number of invasive A549 cells to 781.5 ± 28.99, 234 ± 22.71, 108 ± 6.00, 81.33 ± 14.22, and 35.66 ± 2.51 cells per field, respectively

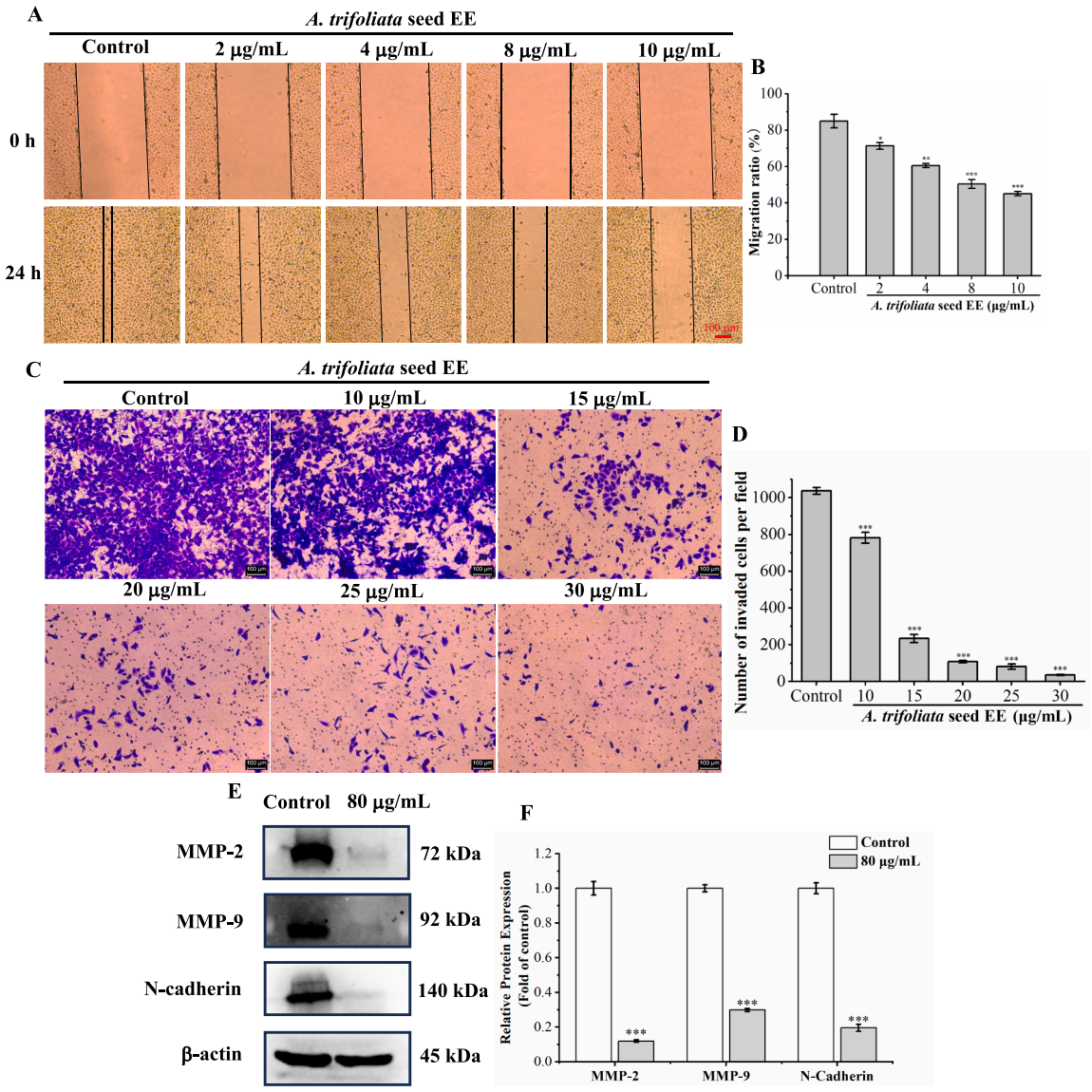

Fig. 8. The effect of *A. trifoliata* seed EE on the migratory and invasive abilities of A549 cells. **(A, B)** Wound healing assay was used to detect the migratory ability of A549 cells, which was quantified using migration rate (%). **(C, D)** Invasive capacity was tested using transwell invasion assay and was quantified using the amount of invasive A549 cells per field. **(E, F)** The metastasis-associated proteins (MMP-2, MMP-9, and N-cadherin) in *A. trifoliata* seed EE-treated A549 cells were detected by western blot. Data were displayed as means ± SD. Bars represent mean values, and error bars represent SD. Statistical significance of wound healing and transwell invasion assay results was determined using one-way analysis of variance (ANOVA) with the LSD. Statistical differences in western blot analysis were determined using the two-tailed unpaired *t*-test. $^{*}p < 0.05$, $^{**}p < 0.01$, $^{***}p < 0.001$ in comparison to the control group.

(Fig. 8C and D). All these results indicated that *A. trifoliata* seed EE dose-dependently depressed the migratory and invasive abilities of the A549 cell line.

Western blot was used to determine the impact of *A. trifoliata* seed EE on metastasis-associated proteins (Fig. 8E and F). *A. trifoliata* seed EE significantly down-regulated MMP-2, MMP-9, and N-cadherin levels. All the above results suggested that *A. trifoliata* seed EE depressed the levels of MMP-2, MMP-9, and N-cadherin, thereby inhibiting the migratory and invasive abilities of A549 cells.

4. Discussion

According to the MTT results, *A. trifoliata* seed EE exhibited selective cytotoxicity, showing high toxicity to A549 cells and low toxicity to non-cancerous cells (MRC-5 and L929). Anticancer drugs with selective cytotoxicity to cancer cells and low toxicity to non-cancer cells have great advantages in cancer therapy and are ideal anticancer drugs (Blagosklonny, 2004; Pawlak et al., 2022). Past studies have demonstrated that *A. trifoliata* seed ethanolic extract significantly suppressed the viability of hepatocellular carcinoma HepG2, HuH7, and SMMC-7721 cells with IC_{50} values of 2.61 mg/mL, 2.27 mg/mL, and 2.63 mg/mL, respectively (Lu et al., 2014; Lu et al., 2019). In addition, gastric cancer SGC-7901 cells were treated with ethanol extract of *A. trifoliata* seed at a concentration of 2.5 g/mL for 48 h, and cell viability was suppressed with an inhibition rate of 56.9 ± 5.3 % (Lu et al., 2013). Moreover, *A. trifoliata* stem ethanol extract showed remarkable cytotoxicity against hepatocellular carcinoma SMMC-7721 (IC_{50}: 0.355 mg/mL), BEL-7404 cells (IC_{50}: 0.368 mg/mL), and human nasopharyngeal carcinoma CNE-1 cells (IC_{50}: 0.192 mg/mL) (Tang et al., 2014). Comparing the above studies, we also found that *A. trifoliata* seed EE had significant cytotoxicity to lung cancer cells.

Based on UHPLC-Q-Orbitrap-MS analysis, 44 compounds were identified in EE. Subsequently, we employed network pharmacology to further analyze the anti-tumor mechanisms of these chemical

components identified in *A. trifoliata* seed EE (Fig.S1, Supplementary Material). A total of 7 potential active components (2-isopropylmalic acid, procyanidin B1, (+)-catechin hydrate, leucinic acid, morin, kaempferol, and quercetin) and 6 core target proteins (CDK2, caspase 3, MMP-9, Bcl-2, PARP1, and MMP-2) were screened out (Fig. S1, Supplementary Material). Further validation of the binding of the active components and target proteins was achieved by molecular docking (Fig. S3, Supplementary Material). If the binding affinity is less than −5 kcal/mol, this indicates a potent binding activity. As summarized in Table S1, the binding energies of CDK2 to 2-isopropylmalic acid, (+)-catechin hydrate, kaempferol, morin, procyanidin B1, quercetin, and leucinic acid were −7.13, −6.61, −7.32, −7.13, −6, −6.91, and −5.46 kcal/mol, respectively. The binding energies of caspase 3 to these active components were as follows: −5.85 kcal/mol (2-isopropylmalic acid), −6.3 kcal/mol ((+)-catechin hydrate), −6.41 kcal/mol (kaempferol), −6.77 kcal/mol (morin), −6.18 kcal/mol (procyanidin B1), −6.22 kcal/mol (quercetin), and −5.02 kcal/mol (leucinic acid). Besides, the binding energies of MMP-9 with (+)-catechin hydrate, kaempferol, leucinic acid, procyanidin B1, quercetin, and morin were −6.25, −6.7, −5.56, −5.6, −6.08, and −6.46 kcal/mol, respectively. Bcl-2 was shown to bind (+)-catechin hydrate, kaempferol, morin, quercetin, and procyanidin B1 with binding energies of −6.84, −6.18, −6.27, −6.24, and −5.24 kcal/mol, respectively. Additionally, (+)-catechin hydrate, kaempferol, morin, quercetin, and procyanidin B1 bound PARP1 with binding energies of −7.21, −7.04, −7.02, and −6.34 kcal/mol, respectively. MMP-2 bound to these active ingredients with the following energies: −6.91 kcal/mol ((+)-catechin hydrate), −5.44 kcal/mol (kaempferol), −5.06 kcal/mol (morin), and −5.11 kcal/mol (quercetin).

CDK2 plays an essential role in controlling the cell cycle, regulating the transition from the G1 phase to the S phase and the progression of the S phase (Zhu et al., 2021). Caspase 3 is a well-established apoptosis marker and activated caspase 9 that catalyzes the cleavage of multiple key proteins and executes the apoptotic process (Altyar and Fahmy, 2022; Laghezza Masci et al., 2020). MMP-2 and MMP-9 belong to the matrix metalloproteinase family and affect cancer cell metastasis by degrading type IV collagen in the basement membrane (Gu, 2018). Bcl-2, an early identified anti-apoptotic protein, plays an important role in cell apoptosis (Kang et al., 2021). PARP1 regulates cancer-related biological processes, such as apoptosis (Wang et al., 2017). Consequently, *A. trifoliata* seed EE may regulate these six targets (CDK2, caspase 3, MMP-9, Bcl-2, PARP1, and MMP2) to affect A549 cell proliferation, apoptosis, and metastasis.

Uncontrolled malignant proliferation of cancer cells is mainly caused by cell cycle disorder (Chen et al., 2021a). Our findings demonstrated that *A. trifoliata* seed EE suppressed A549 cell proliferation by blocking the cell cycle in the S phase in colony formation and cell cycle analysis. Previous research has demonstrated that cyclin E regulates the transition from the G1 phase to the S phase (Siu et al., 2012). CDK2 is generally considered essential for S-phase progression (Liu et al., 2018a). The p21 inhibits cell cycle progression by arresting the cell cycle in the G1 phase (Giordano et al., 2023). Therefore, our study detected the levels of CDK2, cyclin E1, p21, and cyclin E2, and the results showed that *A. trifoliata* seed EE enhanced cell percentage in the S phase by up-regulating cyclin E1 and cyclin E2 and down-regulating p21 and CDK2, thus obstructing A549 cell proliferation.

Avoiding cell death is one of the hallmarks of tumors (Sun et al., 2020). A549 cell nuclear and cellular morphology were analyzed based on morphological observations, Hoechst 33,258 staining, and AO/EB staining, which showed typical apoptotic morphological alterations, such as cell rounding, cell shrinkage, and nuclear pyknosis. Further, flow cytometry analysis revealed that *A. trifoliata* seed EE triggered dose-dependently apoptosis in A549 cells. JC-1 assay results revealed that mitochondrial membrane potential (ΔΨm) was reduced by *A. trifoliata* seed EE, resulting in A549 cell apoptosis. The ΔΨm is primarily controlled by Bcl-2 family proteins, which include pro-apoptotic (Bax and Bid) and anti-apoptotic (Bcl-2 and Bcl-xL) (Malyarenko et al., 2017; Tao et al., 2021). By increasing the proportion of Bax/Bcl-2, ΔΨm is down-regulated, and caspase 9 and caspase 3 are activated, resulting in PARP cleavage and eventually inducing apoptosis in cancer cells (Chen et al., 2021b). In western blot assay, *A. trifoliata* seed EE raised the Bax/Bcl-2 ratio and lowered ΔΨm, which cleaved and activated caspase 9 and caspase 3, thereby cleaving PARP and resulting in apoptosis in A549 cells. Thus, *A. trifoliata* seed EE triggered apoptosis through the mitochondrial pathway.

The metastatic spread of cancer is the leading cause of cancer death (Darzi et al., 2021). In our study, *A. trifoliata* seed EE remarkably and dose-dependently suppressed A549 cell migratory and invasive capacity. MMP-2 and MMP-9 belong to the matrix metalloproteinase family, degrade collagen type IV (the basement membrane's most plentiful component), and act as a pivotal part of cancer metastasis (Gu, 2018). Since elevated N-cadherin expression is connected to cancer metastasis, lowering N-cadherin level limits cancer metastasis (Cao et al., 2019). Hence, our study examined the expression of N-cadherin, MMP-2, and MMP-9. The results showed that *A. trifoliata* seed EE suppressed A549 cell metastatic ability by down-regulating MMP-2, MMP-9, and N-cadherin expression.

Previous study has demonstrated that morin inhibited the proliferation of human leukemia HL-60 cells by inducing cell cycle arrest (Kuo et al., 2007). By raising the Bax/Bcl-2 ratio, activating caspase 9 and caspase 3, and cleaving PARP, morin caused colorectal cancer SW480 cell apoptosis (Sithara et al., 2017). Additionally, morin inhibited breast cancer MDA-MB-231 cell metastasis by lowering MMP-9 and N-cadherin expression (Jin et al., 2014). Kaempferol arrested colorectal cancer HT-29 cell cycle by decreasing CDK2 and cyclin E levels, thereby inhibiting HT-29 cell proliferation (Cho and Park, 2013). Furthermore, kaempferol's impact on apoptosis was verified in A549 cells, where it increased Bax levels, triggered caspase 3 and caspase 9 activation, and cleaved PARP (Nguyen et al., 2003; Qin et al., 2016). Kaempferol lowered A549 cell metastatic capacity by suppressing N-cadherin expression (Jo et al., 2015). Quercetin has been discovered to restrain metastasis by suppressing MMP-9, MMP-2, and N-cadherin expression in A549 cells, inhibit proliferation by triggering S-phase arrest, and induce apoptosis by elevating the ratio of Bax to Bcl-2 and triggering caspase 9 and caspase 3 activation (Elumalai et al., 2022; Guo et al., 2021; Lee et al., 2008; Nguyen et al., 2004; Yang et al., 2022). Procyanidin B1 triggered apoptosis by regulating mitochondrial apoptotic pathway-linked proteins (Bax, Bcl-2, and caspase 3) and suppressed the proliferation of colorectal cancer HCT-116 and SW620 cells by inducing cell cycle arrest (Lei et al., 2023). Additionally, procyanidin B1 has been demonstrated to suppress metastasis in liver cancer cells (HepG2, HuH-7) (Na et al., 2020). (+)-Catechin hydrate suppressed cancer cell proliferation and induced apoptosis *via* regulating caspase 9 and caspase 3 levels in cervical cancer SiHa cells and breast cancer MCF-7 cells (Al-Hazzani and Alshatwi, 2011; Alshatwi, 2010). Therefore, these compounds may play an important role in the antiproliferative, apoptosis-inducing, and metastasis-inhibiting effects of *A. trifoliata* seed EE on A549cells.

Previous studies have found that *A. trifoliata* seed ethanol extract effectively inhibited hepatocellular carcinoma cell proliferation by inducing endoplasmic reticulum stress (Lu et al., 2014). In addition, *A. trifoliata* seed ethanol extract suppressed the metastasis of hepatocellular carcinoma cells by downregulating MMP-2, MMP-9, and N-cadherin levels (Lu et al., 2019). Various triterpenoids from *A. trifoliata* stem induced apoptosis *via* activation of caspase 3 and caspase 7 in pig kidney LLC-PK1 cells (Pawar et al., 2006). In the European Pharmacopoeia, the '*Akebia* stem' monograph allows the use of *Akebia quinata*, *Akebia trifoliata*, or a mixture of the two species as a raw material (Maciąg et al., 2021). Multiple active ingredients from *A. quinata*, like polysaccharides and saponins, induced apoptosis and suppressed metastasis in hepatocellular carcinoma cells and breast cancer cells (An et al., 2016; Kang et al., 2010; Wang et al., 2023). Our study also demonstrated that *A. trifoliata* seed EE suppressed proliferation, induced

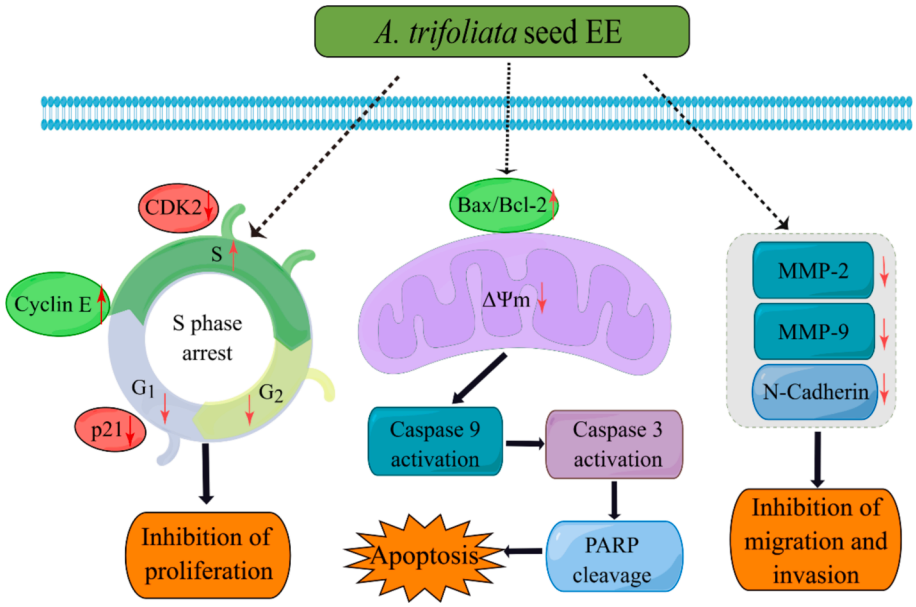

Fig. 9. Predicting anticancer mechanism of *A. trifoliate* seed EE in antiproliferation, apoptosis induction, and metastasis inhibition in A549 cells.

apoptosis, and inhibited metastasis in lung cancer A549 cells.

In China, multiple plant extracts have been developed into anticancer drugs for clinical use, like *Xiaoaiping* injection (*Marsdenia tenacissima* water extract), *Hedyotis diffusa* injection (*Hedyotis diffusa* ethanolic extract), and *Brucea javanica* oil soft capsule (*Brucea javanica* petroleum ether extract) (Huang et al., 2022; Zhang et al., 2018; Zhou et al., 2022a). Therefore, plant-derived extracts can serve as an important source of anticancer drugs. The entire fruit of *A. trifoliata*, including the seed, has been included in the Chinese Pharmacopoeia for the treatment of cancer (China Pharmacopoeia Committee, 2020; Tang et al., 2020). Our findings demonstrate that *A. trifoliata* seed EE has excellent anti-lung cancer effects *in vitro*, which promotes its development and utilization in the pharmaceutical industry. However, its anti-lung cancer effects *in vivo* still require further study.

In conclusion, *A. trifoliata* seed EE restrained proliferation, induced apoptosis *via* the mitochondrial pathway, and suppressed the migratory and invasive abilities of A549 cells. As illustrated in Fig. 9, *A. trifoliata* seed EE blocked the cell cycle in the S phase, which suppressed A549 cell proliferation. At the same time, it increased the Bax/Bcl-2 ratio, reduced ΔΨm, activated caspase 9 and caspase 3, cleaved PARP, and then triggered apoptosis through the mitochondrial pathway. *A. trifoliata* seed EE repressed A549 cell migratory and invasive abilities by down-regulating N-cadherin, MMP-9, and MMP-2. The evidence indicates that *A. trifoliata* seed EE exhibits anticancer properties *in vitro*, which provides the basis for the exploitation of *A. trifoliata* seed EE as an anticancer drug in the pharmaceutical industry.

5. Conclusion

A. trifoliata fruit is used to treat tumors, and the seed makes up more than 50 % of the fruit weight. However, *A. trifoliata* seed is usually discarded as waste, and its anti-tumor effect remains poorly studied. Therefore, we focused on *A. trifoliata* seed and investigated its anti-lung cancer properties and associated mechanisms for the first time. By using UHPLC-Q-Orbitrap-MS, 82 phytochemicals were identified in WE and EE, the majority of which were flavonoids, terpenes, and phenols. *A. trifoliata* seed EE demonstrated selective cytotoxicity with high cytotoxicity to A549 cells and low cytotoxicity to non-cancerous cells (MRC-5 and L929). In addition, *A. trifoliata* seed EE inhibited A549 cell proliferation *via* arresting at the S phase, caused apoptosis through the mitochondrial apoptosis pathway, and inhibited migratory and invasive abilities. Hence, *A. trifoliata* seed EE exhibits outstanding anticancer properties and has the potential to be exploited as an anticancer drug in the pharmaceutical industry.

CRediT authorship contribution statement

Yuanquan Ran: Writing – original draft, Methodology, Investigation. **Lanlan Yang:** Methodology, Investigation. **Xiaoyan Jia:** Methodology, Investigation. **Huan Zhao:** Validation, Software. **Qiong Hu:** Validation. **Bing Yang:** Validation. **Dongxin Tang:** Writing – review & editing, Funding acquisition, Conceptualization. **Minyi Tian:** Writing – review & editing, Writing – original draft, Validation, Supervision, Methodology, Funding acquisition.

Declaration of competing interest

The authors declare that they have no known competing financial interests or personal relationships that could have appeared to influence the work reported in this paper.

Acknowledgments

The authors are grateful for the financial support grant from the National Natural Science Foundation of China (82360834 and 82260957) and the Guizhou Provincial Higher Education Traditional Chinese and Medicine Ethnic Medicine Cancer Prevention and Treatment Medical Transformation Engineering Research Center, China (Qian Jiaoji [2023]037).

Appendix A. Supplementary data

Supplementary data to this article can be found online at https://doi.org/10.1016/j.arabjc.2024.106020.

References

Al-Hazzani, A.A., Alshatwi, A.A., 2011. Catechin hydrate inhibits proliferation and mediates apoptosis of SiHa human cervical cancer cells. Food. Chem. Toxicol. 49, 3281–3286.

Alshatwi, A.A., 2010. Catechin hydrate suppresses MCF-7 proliferation through TP53/Caspase-mediated apoptosis. J. Exp. Clin. Cancer. Res. 29, 167.

Altyar, A.E., Fahmy, O., 2022. Preparation of liposomal raloxifene-graphene nanosheet and evaluation of Its *In Vitro* anticancer effects. Dose. Response. 20, 1–10.

An, J.P., Ha, T.K., Kim, J., Cho, T.O., Oh, W.K., 2016. Protein Tyrosine Phosphatase 1B Inhibitors from the Stems of *Akebia quinata*. Molecules 21, 1091.
Blagosklonny, M.V., 2004. Analysis of FDA approved anticancer drugs reveals the future of cancer therapy. Cell Cycle 3 (8), 1035–1042.
Cao, Z.Q., Wang, Z., Leng, P., 2019. Aberrant N-cadherin expression in cancer. Biomed. Pharmacother. 118, 109320.
Chen, D., Tatemi, S., 2001. Lardizabalaceae. In: Wu, Z.Y., Raven, P.H. (Eds.), Flora of China, Vol. 6. Science Press, Beijing & Missouri Botanical Garden Press, St. Louis, pp. 440–454.
Chen, C., Lv, Q., Li, Y., Jin, Y.H., 2021b. The Anti-Tumor Effect and Underlying Apoptotic Mechanism of Ginsenoside Rk1 and Rg5 in Human Liver Cancer Cells. Molecules 26, 3926.
Chen, F., Song, J., Ye, Z., Xu, B., Cheng, H., Zhang, S., Sun, X., 2021a. Integrated analysis of cell cycle-related and immunity-related biomarker signatures to improve the prognosis prediction of lung adenocarcinoma. Front. Oncol. 11, 666826.
Chen, J., Sun, Z., Chen, J., Luan, M., 2022. Metabolomic Profile and antibacterial bioactivity of *Akebia trifoliata* (Thunb.) koidz pericarp extract. Processes 10, 1394.
Cho, H.J., Park, J.H., 2013. Kaempferol Induces Cell Cycle Arrest in HT-29 Human Colon Cancer Cells. J. Cancer. Prev. 18 (3), 257–263.
China Pharmacopoeia Committee, 2020. Pharmacopoeia of the People's Republic of China, China Medical Science and Technology Press, Beijing, China, vol. 1. pp. 65, 310.
Darzi, M., Gorgin, S., Majidzadeh-A, K., Esmaeili, R., 2021. Gene co-expression network analysis reveals immune cell infiltration as a favorable prognostic marker in non-uterine leiomyosarcoma. Sci. Rep. 11, 2339.
European Commission Database for Information on Cosmetic Substances and Ingredients (CosIng), 2024. Available online: https://ec.europa.eu/growth/tools-databases/cosing/details/54448 (Accessed on 6 May 2024).
El-Hawary, S.S., Mohammed, R., Taher, M.A., AbouZid, S.F., Mansour, M.A., Almahmoud, S.A., Huwaimel, B., Amin, E., 2022. Characterization of Promising Cytotoxic Metabolites from *Tabebuia guayacan* Hemsl.: Computational Prediction and In Vitro Testing. Plants 11, 888.
Elumalai, P., Ezhilarasan, D., Raghunandhakumar, S., 2022. Quercetin Inhibits the Epithelial to Mesenchymal Transition through Suppressing Akt Mediated Nuclear Translocation of β-Catenin in Lung Cancer Cell Line. Nutr. Cancer 74, 1894–1906.
Giordano, F., Paolì, A., Forastiero, M., Marsico, S., De Amicis, F., Marrelli, M., Naimo, G. D., Mauro, L., Panno, M.L., 2023. Valproic acid inhibits cell growth in both MCF-7 and MDA-MB231 cells by triggering different responses in a cell type-specific manner. J. Transl. Med. 21, 165.
Gu, M., 2018. IL13Rα2 siRNA inhibited cell proliferation, induced cell apoptosis, and suppressed cell invasion in papillary thyroid carcinoma cells. Onco. Targets. Ther. 11, 1345–1352.
Guan, J., Fu, P., Wang, X., Yu, X., Zhong, S., Chen, W., Luo, P., 2022. Assessment of the breeding potential of a set of genotypes selected from a natural population of *Akebia trifoliata* (three–leaf Akebia). Horticulturae 8, 116.
Guo, H., Ding, H., Tang, X., Liang, M., Li, S., Zhang, J., Cao, J., 2021. Quercetin induces pro-apoptotic autophagy via SIRT1/AMPK signaling pathway in human lung cancer cell lines A549 and H1299 in vitro. Thorac. Cancer 12, 1415–1422.
Huang, M., Lu, J.J., Ding, J., 2021. Natural products in cancer therapy: past, present and future. Nat. Prod. Bioprospect. 11, 5–13.
Huang, F., Pang, J., Xu, L., Niu, W., Zhang, Y., Li, S., Li, X., 2022. *Hedyotis diffusa* injection induces ferroptosis via the Bax/Bcl2/VDAC2/3 axis in lung adenocarcinoma. Phytomedicine 104, 154319.
Jiang, Y., Yin, H., Zheng, Y., Wang, D., Liu, Z., Deng, Y., Zhao, Y., 2020. Structure, physicochemical and bioactive properties of dietary fibers from *Akebia trifoliata* (Thunb.) Koidz. seeds using ultrasonication/shear emulsifying/microwave-assisted enzymatic extraction. Food. Res. Int. 136, 109348.
Jin, H., Lee, W.S., Eun, S.Y., Jung, J.H., Park, H.S., Kim, G., Choi, Y.H., Ryu, C.H., Jung, J.M., Hong, S.C., Shin, S.C., Kim, H.J., 2014. Morin, a flavonoid from Moraceae, suppresses growth and invasion of the highly metastatic breast cancer cell line MDA-MB-231 partly through suppression of the Akt pathway. Int. J. Oncol. 45, 1629–1637.
Jo, E., Park, S.J., Choi, Y.S., Jeon, W.K., Kim, B.C., 2015. Kaempferol Suppresses Transforming Growth Factor-β1-Induced Epithelial-to-Mesenchymal Transition and Migration of A549 Lung Cancer Cells by Inhibiting Akt1-Mediated Phosphorylation of Smad3 at Threonine-179. Neoplasia 17 (7), 525–537.
Kang, E.J., Cho, S., Lim, C., Lee, B., Kim, Y.K., Kim, K.M., 2021. Effects of the methanol fraction of modified Seonghyangjeongki-san water extract on transient ischaemic brain injury in mice. Pharm. Biol. 59 (1), 838–851.
Kang, H.S., Kang, J.S., Jeong, W.S., 2010. Cytotoxic and apoptotic effects of saponins from *Akebia quinata* on HepG2 hepatocarcinoma cells. Korean J. Food Preserv. 17 (3), 311–319.
Kuo, H.M., Chang, L.S., Lin, Y.L., Lu, H.F., Yang, J.S., Lee, J.H., Chung, J.G., 2007. Morin inhibits the growth of human leukemia HL-60 cells via cell cycle arrest and induction of apoptosis through mitochondria dependent pathway. Anticancer. Res. 27, 395–405.
Laghezza Masci, V., Ovidi, E., Taddei, A.R., Turchetti, G., Tiezzi, A., Giacomello, P., Garzoli, S., 2020. Apoptotic Effects on HL60 Human Leukaemia Cells Induced by Lavandin Essential Oil Treatment. Molecules 25, 538.
Lee, J.H., Hong, S.H., Han, M.H., Jin, C.Y., Choi, B.T.C.Y.H., 2008. Apoptosis by Quercetin through induction of Bax and activation of Caspase in human lung carcinoma cells. Caner. Prev. Res. 13 (3), 169–176.
Lei, Y., Deng, X., Zhang, Z., Chen, J., 2023. Natural product procyanidin B1 as an antitumor drug for effective therapy of colon cancer. Exp. Ther. Med. 26, 506.
Lei, L., Zhao, Q., Selomulya, C., Xiong, H., 2015. The effect of deamidation on the structural, functional, and rheological properties of glutelin prepared from *Akebia trifoliata* var. australis seed. Food. Chem. 178, 96–105.
Li, X., Wei, J., Lin, L., Li, J., Zheng, G., 2023a. Structural characterization, antioxidant and antimicrobial activities of polysaccharide from *Akebia trifoliata* (Thunb.) Koidz stem. Colloids. Surf. b. Biointerfaces 231, 113573.
Li, X., Wei, J., Lin, L., Zheng, G., 2023b. Extraction, moisturizing activity and potential application in skin cream of *Akebia trifoliata* (Thunb.) Koidz polysaccharide. Ind. Crop. Prod. 197, 116613.
Li, L., Yao, X., Zhong, C., Chen, X., Huang, H., 2010. Akebia: A potential new fruit crop in China. HortSci. 45 (1), 4–10.
Liu, Y.C., Wang, H.M., Zeng, X.H., 2018b. Research progress of active compounds and pharmacological effects in *Akebia trifoliata* (Thunb) koidz stems. IOP. Conf. Ser. Earth. Environ. Sci. 185, 012034.
Liu, O.G., Xiong, X.Y., Li, C.M., Zhou, X.S., Li, S.S., 2018a. Role of Xeroderma Pigmentosum Group D in Cell Cycle and Apoptosis in Cutaneous Squamous Cell Carcinoma A431 Cells. Med. Sci. Monit. 24, 453–460.
Lu, W.L., Ren, H.Y., Liang, C., Zhang, Y.Y., Xu, J., Pan, Z.Q., Liu, X.M., Wu, Z.H., Fang, Z. Q., 2014. *Akebia trifoliate* (Thunb.) Koidz Seed Extract Inhibits the Proliferation of Human Hepatocellular Carcinoma Cell Lines *via* Inducing Endoplasmic Reticulum Stress. Evid. Based Complement. Alternat. Med. 2014, 192749.
Lu, W.L., Yang, T., Song, Q.J., Fang, Z.Q., Pan, Z.Q., Liang, C., Jia, D.W., Peng, P.K., 2019. *Akebia trifoliata* (Thunb.) Koidz Seed Extract inhibits human hepatocellular carcinoma cell migration and invasion in vitro. J. Ethnopharmacol. 234, 204–215.
Lu, Y.Z., Ye, H.M., Zeng, H.Z., Li, L.H., Wu, G.Y., Liu, G.Y., 2013. A study on the extraction process of active ingredients from *Akebia stem* and an analysis of their anti-gastric cancer activity. Afr. J. Tradit. Complement. Altern. Med. 10 (5), 313–317.
Maciąg, D., Dobrowolska, E., Sharafan, M., Ekiert, H., Tomczyk, M., Szopa, A., 2021. *Akebia quinata* and *Akebia trifoliata* - a review of phytochemical composition, ethnopharmacological approaches and biological studies. J. Ethnopharmacol. 280, 114486.
Malyarenko, O.S., Dyshlovoy, S.A., Kicha, A.A., Ivanchina, N.V., Malyarenko, T.V., Carsten, B., Gunhild, V.A., Stonik, V.A., Ermakova, S.P., 2017. The Inhibitory Activity of Luzonicosides from the Starfish *Echinaster luzonicus* against Human Melanoma Cells. Mar. Drugs 15, 227.
Min, W., Qu, D., Lin, F., Li, H., Peng. J., Zhang, Q., 2023. Investigation and performance evaluation of skin cream with *Akebia trifoliata* (Thunb) seed oil. Guangzhou Chem. Ind. 51 (10), 70–72+101.
Na, W., Ma, B., Shi, S., Chen, Y., Zhang, H., Zhan, Y., An, H., 2020. Procyanidin B1, a novel and specific inhibitor of Kv10.1 channel, suppresses the evolution of hepatoma. Biochem. Pharmacol. 178, 114089.
Naeem, A., Hu, P., Yang, M., Zhang, J., Liu, Y., Zhu, W., Zheng, Q., 2022. Natural Products as Anticancer Agents: Current Status and Future Perspectives. Molecules 27, 8367.
National Medical Products Administration (NMPA), 2024. Catalogue of Cosmetic Raw Materials Used (2021 Edition). Available online: https://www.nmpa.gov.cn/xxgk/ggtg/hzhpggtg/jmhzhptg/20210430162707173.html (Accessed on 06 May 2024).
Nguyen, T.T., Tran, E., Ong, C.K., Lee, S.K., Do, P.T., Huynh, T.T., Nguyen, T.H., Lee, J.J., Tan, Y., Ong, C.S., Huynh, H., 2003. Kaempferol-induced growth inhibition and apoptosis in A549 lung cancer cells is mediated by activation of MEK-MAPK. J. Cell. Physiol. 197, 110–121.
Nguyen, T.T., Tran, E., Nguyen, T.H., Do, P.T., Huynh, T.H., Huynh, H., 2004. The role of activated MEK-ERK pathway in quercetin-induced growth inhibition and apoptosis in A549 lung cancer cells. Carcinogenesis 25 (5), 647–659.
Niu, J., Jia, X., Yang, N., Ran, Y., Wu, X., Ding, F., Tang, D., Tian, M., 2024. Phytochemical analysis and anticancer effect of *Camellia oleifera* bud ethanol extract in non-small cell lung cancer A549 cells. Front. Pharmacol. 15, 1359632.
Ouyang, J.K., Dong, L.M., Xu, Q.L., Wang, J., Liu, S.B., Qian, T., Yuan, Y.F., Tan, J.W., 2018. Triterpenoids with α-glucosidase inhibitory activity and cytotoxic activity from the leaves of *Akebia trifoliata*. RSC. Adv. 8 (70), 40483–40489.
Pawar, R.S., Balachandran, P., Pasco, D.S., Khan, I.A., 2006. Cytotoxicity studies of triterpenoids from *Akebia trifoliata* and *Clematis ligusticifolia*. Acta. Hortic. 720, 171–178.
Pawlak, A., Chybicka, K., Zioło, E., Strządała, L., Kałas, W., 2022. The Contrasting Delayed Effects of Transient Exposure of Colorectal Cancer Cells to Decitabine or Azacitidine. Cancers 14, 1530.
Qin, Y., Cui, W., Yang, X., Tong, B., 2016. Kaempferol inhibits the growth and metastasis of cholangiocarcinoma in vitro and in vivo. Acta. Bioch. Bioph. Sin. 48 (3), 238–245.
Sithara, T., Arun, K.B., Syama, H.P., Reshmitha, T.R., Nisha, P., 2017. Morin inhibits proliferation of sw480 colorectal cancer cells by inducing apoptosis mediated by reactive oxygen species formation and uncoupling of warburg effect. Front. Pharmacol. 8, 640.
Siu, K.T., Rosner, M.R., Minella, A.C., 2012. An integrated view of cyclin E function and regulation. Cell Cycle 11 (1), 57–64.
Sivandzade, F., Bhalerao, A., Cucullo, L., 2019. Analysis of the Mitochondrial Membrane Potential Using the Cationic JC-1 Dye as a Sensitive Fluorescent Probe. Bio. Protoc. 9 (1), e3128.
Su, S., Wu, J., Peng, X., Li, B., Li, Z., Wang, W., Jian, W., Xu, X., 2021. Genetic and agro-climatic variability in seed fatty acid profiles of *Akebia trifoliata* (Lardizabalaceae) in China. J. Food. Compos. Anal. 102, 104064.
Sun, G., Ding, X.A., Argaw, Y., Guo, X., Montell, D.J., 2020. Akt1 and dCIZ1 promote cell survival from apoptotic caspase activation during regeneration and oncogenic overgrowth. Nat. Commun. 11, 5726.
Sun, X.D., Zhang, X.W., Tan, S., 2018. Processing technology optimization of *Akebia trifoliata* peel tea. Guizhou. Agr. Sci. 46 (11), 134–137+141.

Sung, H., Ferlay, J., Siegel, R.L., Laversanne, M., Soerjomataram, I., Jemal, A., Bray, F., 2021. Global Cancer Statistics 2020: GLOBOCAN Estimates of Incidence and Mortality Worldwide for 36 Cancers in 185 Countries. CA. Cancer. J. Clin. 71, 209–249.

Tang, D.X., Long, F.X., 2020. Collection of Miao Anti-tumor Drugs [*Miaozu Kangzhongliu Yaowuji*], China Press of Traditional Chinese Medicine Co., Ltd, Beijing. China, pp.21–23.

Tang, Y., Sun, Y., Liang, G., 2014. Anti-tumor active of the ethanol extract from *Akebia trifoliata* in Vitro. Chinese J. Ethnomed. Ethnoph. 23 (10), 17–18.

Tao, L., Yin, Z., Ni, T., Chu, Z., Hao, S., Wang, Z., Sunagawa, M., Wang, H., Liu, Y., 2021. The Ethyl Acetate Extract from *Celastrus orbiculatus* Promotes Apoptosis of Gastric Cancer Cells Through Mitochondria Regulation by PHB. Front. Pharmacol. 12, 635467.

Wang, L., Liang, C., Li, F., Guan, D., Wu, X., Fu, X., Lu, A., Zhang, G., 2017. PARP1 in Carcinomas and PARP1 Inhibitors as Antineoplastic Drugs. Int. J. Mol. Sci. 18, 2111.

Wang, H., Lin, Z., Li, Y., Wang, X., Xu, J., Guo, Y., 2023. Characterization, selenylation, and antineoplastic effects on HepG2 cells in vitro and in vivo of an arabinofuranan from the fruits of *Akebia quinata*. Arab. J. Chem. 16, 104448.

WFO, 2024. *Akebia trifoliata* (Thunb.) Koidz. Published on the Internet: https://www.worldfloraonline.org/taxon/wfo-0000524892 (Accessed on 06 May 2024).

Yang, P., Li, X., Wen, Q., Zhao, X., 2022. Quercetin attenuates the proliferation of arsenic-related lung cancer cells via a caspase-dependent DNA damage signaling. Mol. Carcinog. 61 (7), 655–663.

Yu, Y.Q., Thonn, V., Patankar, J.V., Thoma, O.M., Waldner, M., Zielinska, M., Bao, L.L., Gonzalez-Acera, M., Wallmüller, S., Engel, F.B., Stürzl, M., Neurath, M.F., Liebing, E., Becker, C., 2022. SMYD2 targets RIPK1 and restricts TNF-induced apoptosis and necroptosis to support colon tumor growth. Cell Death Dis. 13, 52.

Yu, N., Wang, X., Ning, F., Jiang, C., Li, Y., Peng, H., Xiong, H., 2019. Development of antibacterial pectin from *Akebia trifoliata* var. australis waste for accelerated wound healing. Carbohyd. Polym. 217, 58–68.

Zhang, Z., Yang, F., Liu, H., Xu, G., Zhu, Q., Yu, L., Liao, S., 2024. Chemical Composition and α-Glucosidase Inhibitory of the Seeds of *Akebia trifoliata*. Mod. Food Sci. Technol. 40 (11), 1–9.

Zhang, Y., Zhang, L., Zhang, Q., Zhang, X., Zhang, T., Wang, B., 2018. Enhanced gastric therapeutic effects of *Brucea javanica* oil and its gastroretentive drug delivery system compared to commercial products in pharmacokinetics study. Drug Des. Dev. Ther. 12, 535–544.

Zhou, X.Q., Chang, Y.Z., Shen, C.Y., Han, J., Chang, R.A., 2022a. Xiaoaiping injection combined with chemotherapy for advanced gastric cancer: An updated systematic review and meta-analysis. Front. Pharmacol. 13, 1023314.

Zhou, Y., Jie, B., Wu, G., Cao, Y., Wu, W., Meng, H., 2017. Research progress of *Akebia trifoliata* (Thunb.) Koidz. Agric. Biotechnol. 6 (6), 1–8.

Zhou, J., Shu, Y., Guo, Y., Zhou, X., 2022b. Preparation and evaluation of handmade soap from august melon. Guangzhou Chem. Ind. 50 (17), 72–74.

Zhu, Y., Wang, A., Li, R., Zhu, H., Hu, L., Chen, W., 2021. Total ginsenosides promote the IEC-6 cell proliferation via affecting the regulatory mechanism mediated by polyamines. Saudi Pharm. J. 29, 1223–1232.

Zou, S., Gao, P., Jia, T., Huang, H., 2022. Physicochemical characteristics and nutritional composition during fruit ripening of *Akebia trifoliata* (Lardizabalaceae). Horticulturae 8, 326.